Design of the Energy Structures of Photovoltaic Organic Co-deposited Films by Impurity Doping

2013

Norihiro Ishiyama

Preface

This thesis was performed under the guidance of Professor Masahiro Hiramoto at Department of Functional Molecular Science, School of Physical Sciences, The Graduate University for Advanced Studies.

The aim of this work is to develop doping technique in order to design the appropriate energy structures of photovoltaic co-deposited films for high efficient organic solar cells.

The author believes that techniques developed in this thesis will lead to the development of a high-efficient organic solar cell.

Norihiro Ishiyama

Department of Functional Molecular Science

School of Physical Sciences

The Graduate University for Advanced Studies

March 2013

Contents

Chapter 1:

General Introduction

1.1. Background

Currently, problems related to energy generation have been increasing all over the world. Since electrical power has traditionally been generated using fossil fuels such as oil, coal, and natural gas over the long term, these non-renewable resources are drying up. In addition, nuclear fuel, which has been used as an alternative energy resource, carries with it the serious risk of environmental pollution. Therefore, renewable and clean energy sources must be developed as rapidly as possible.

Photovoltaic energy conversion, which can generate direct-current electricity from solar radiation by utilizing solar cells, is a possible candidate to replace the conventional power generation systems. Photovoltaic systems are superior to the conventional systems in many ways, such as the free energy source supplied from the sun, freedom of location, and environmental harmony. However, conventional solar cells consisting of crystalline silicon or gallium compounds are too expensive to become universally applied. Hence, low-cost solar cells must be developed.

Organic solar cells, which consist of thin films of organic semiconductor material produced by printing or vacuum deposition at low temperature, are one example of such a low-cost cell. They have many advantages over conventional inorganic cells, including their light-weight properties and ease of manufacture by ‘roll-to-roll’ printing onto flexible plastic sheets. Therefore, organic solar cells have the potential to be applied to many different fields, such as mobile devices, ‘wrap’

advertising applications, and building components. However, the photoelectric conversion efficiency of organic solar cells is still lower than that of conventional cells.[1] For commercial use, the efficiency must be improved by making a breakthrough in the design of the structures of these cells.

1.2. Overview of this Thesis

This thesis focused on organic solar cells consisting of vacuum-deposited films. Most recent cells include co-deposited films, which consist of two kinds of organic semiconductors, in order to generate significant photocurrent densities. On the other hand, doping-based control of the energy structures of organic solar cells is a significant challenge, as it is in the case of inorganic cells. In particular, there has been no attempt to control the *pn*-properties of organic co-deposited films by doping.

In this thesis, the author developed doping techniques in order to design the energy structures of photovoltaic organic co-deposited films.

A co-deposited film consisting of fullerene and α-sexithiophene (C_{60}:6T), which shows a large open circuit voltage reaching 0.8 V, was used.[2,3] Molybdenum oxide (MoO_3)[4,5,6] and (Cs_2CO_3)[7,8] were used as the acceptor and donor dopants, respectively. In order to dope into the co-deposited films, the author developed a 'three component co-evaporation' technique, in which three different evaporation sources were used. Precise monitoring of the deposition rates of the dopants using a computer monitoring system enabled us to dope as low as 40 ppm by volume concentration. In order to clarify the operation mechanisms of doped junctions,

‘energy-band mapping’ using Kelvin probe and capacitance measurements was employed.

The *pn*-properties of C_{60}:6T co-deposited films could be completely controlled by doping with MoO_3 and Cs_2CO_3. A series of fundamental doped junctions, that is, *p*-type and *n*-type Schottky junctions, *pn*, p^+in^+, and ohmic n^+p^+ homojunctions, and ohmic junctions between metal electrodes and heavily doped p^+ and n^+ layers were fabricated. Based on these doping techniques, a tandem organic solar cell was formed in a C_{60}:6T co-deposited film by connecting two photoactive p^+in^+-homojunctions with an n^+p^+-ohmic interlayer. The open circuit voltage and the conversion efficiency of the tandem cell reached 1.69 V and 2.4%, respectively.

1.3. History of Organic Photovoltaic Cells

Although research into organic photovoltaic cells started in 1958,[9] early cells, which consisted of single molecular layers, generated very little photocurrent.[10,11] In 1986, Tang developed a *pn*-heterojunction cell consisting of copper phthalocyanine (CuPc) and perylene-derivative (Im-PTC) films (**Fig. 1.1(a)**).[12] For this cell, the short-circuit photocurrent density (J_{sc}) and the conversion efficiency were 2.3 mA cm^{-2} and 1% respectively under simulated solar light, which were much larger than the values reported previously. Since donor/acceptor (D/A) sensitization (see also **section 1.4**) was induced, the efficiency of free-carrier generation was considerably increased. However, a significant problem still remained in terms of the cell structure. Since the diffusion length of excitons in organic semiconductors is as short as several nanometers, only excitons generated in a narrow area (around 10 nm) adjacent to the D/A interface

can reach the site where dissociation occurs.[13] Namely, excitons generated in regions distant from the D/A interface cannot be dissociated. Thus, regions that are remote from the D/A interface become 'dead layers' that do not generate photocurrent. Ten nanometer-thick layers were too narrow to absorb sufficient photons to generate significant photocurrent densities.

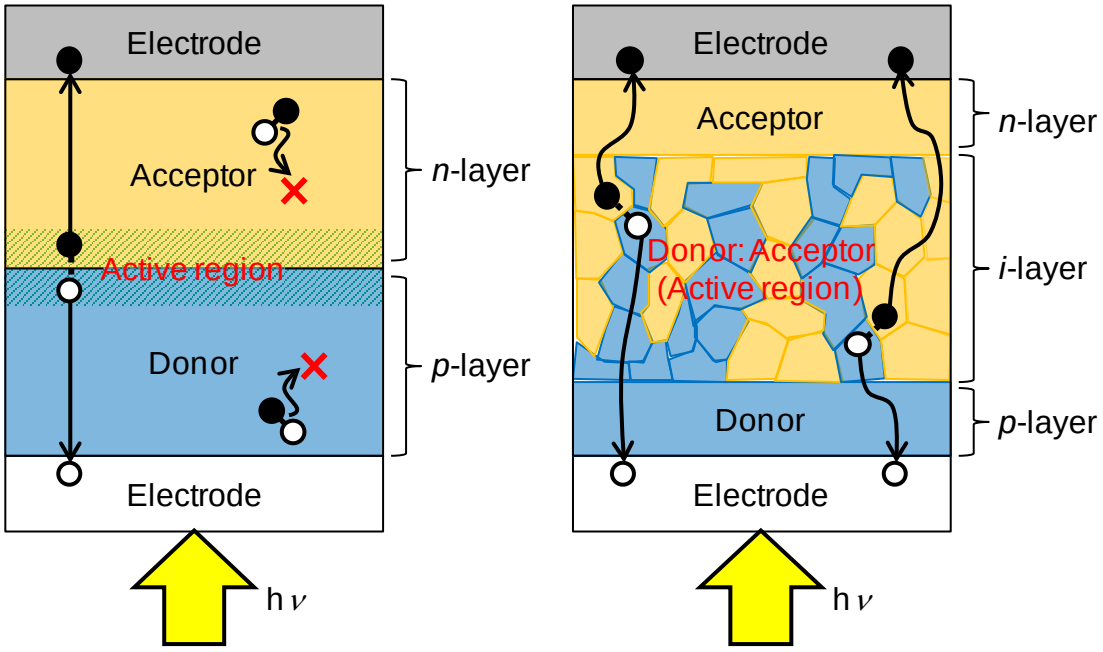

(a) *pn*-Heterojunction cell (b) *pin*-Heterojunction cell

Fig. 1.1 Structures of Donor/Acceptor heterojunction cells and carrier transport mechanisms.

In 1991, Hiramoto et al. proposed a *pin*-heterojunction cell that incorporated a co-deposited film consisting of metal-free phthalocyanine and a perylene derivative (H_2Pc:Me-PTC) (**Fig. 1.1(b)**).[14,15] In the case of the *pin* cell, the value of J_{sc} was almost doubled compared to that of the *pn*-heterojunction cell. Since the molecules of H_2Pc and Me-PTC are mixed on the nanoscale, there are in effect D/A interfaces throughout the whole of the H_2Pc:Me-PTC co-deposited films. That is, photocurrent could be generated within the whole of the co-deposited film, which therefore absorbs a significant portion of the incident light. Thus, the active region for photocurrent generation could be extended by forming a *pin*-heterojunction cell.

Since then, many researchers have attempted to improve the photovoltaic performance of *pin*-heterojunction cells. Peumans et al. demonstrated control of the morphology of a D/A co-deposited film by annealing.[16] On the other hand, Taima et al. reported on the need for optimizing the film thickness of each layer.[17] In addition, there have been many efforts to improve the fabrication processes in order to enhance the efficiency of *pin*-heterojunction cells.[18-22]

Organic photovoltaic materials have also been actively researched (**Fig. 1.2**). Early cells used perylene derivatives as acceptor materials.[12-16] In 1993, N. S. Sariciftci et al. reported that fullerene (C_{60}) acted as an excellent acceptor material.[23] Currently, C_{60}[2,17-22,24-30] and C_{70}[3,31] have become the fundamental acceptor materials of choice. Many different materials have been developed as donor materials to enhance the conversion efficiency. In order to generate significantly high J_{sc} values of more than 10 mA cm^{-2}, materials such as phthalocyanines that possess high absorption-coefficients have been used.[19-21] In addition, materials that exhibit near-infrared absorption have been used to extend the absorption wavelength

region.[24-26] On the other hand, open-circuit voltage (V_{oc}) is also a key factor that affects the efficiency of solar cells. The absolute value of V_{oc} is limited by the energy difference between the HOMO level of the donor and the LUMO level of the acceptor (HOMO-LUMO gap) (**Fig. 1.3**). Since the upper edge of the gap is determined by the LUMO of C_{60}, deep-lying HOMO-level donor materials have been investigated. For example, a combination of α-sexithiophene and C_{60}, which has a large HOMO-LUMO gap (**Fig. 1.3(a)**), exhibits a large V_{oc} value of more than 0.7 V, [2] while a combination of H_2Pc and C_{60}, which has a small gap (**Fig. 1.3(b)**), exhibits a V_{oc} value of 0.4 V. So, in order to improve V_{oc} values, conjugated oligothiophenes,[22,27,28] merocyanine dyes,[29] and rubrene[30] have been used as donor materials.

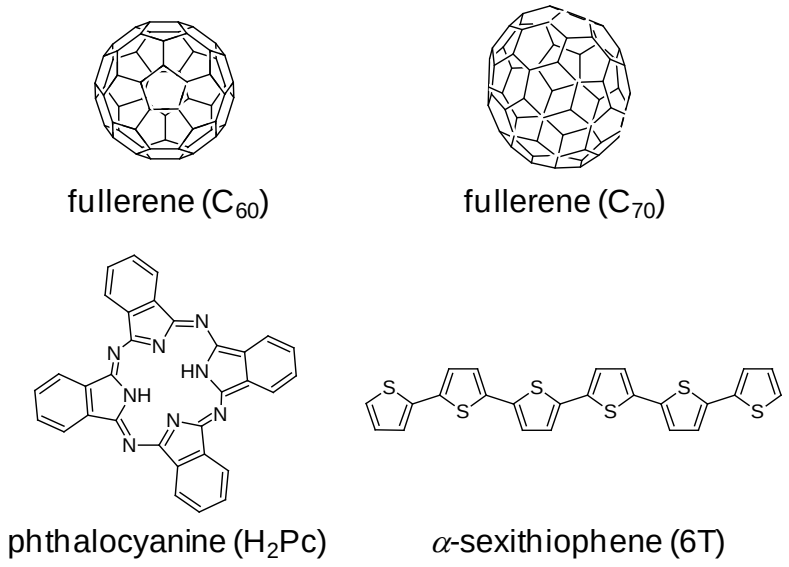

Fig. 1.2 Organic photovoltaic materials.

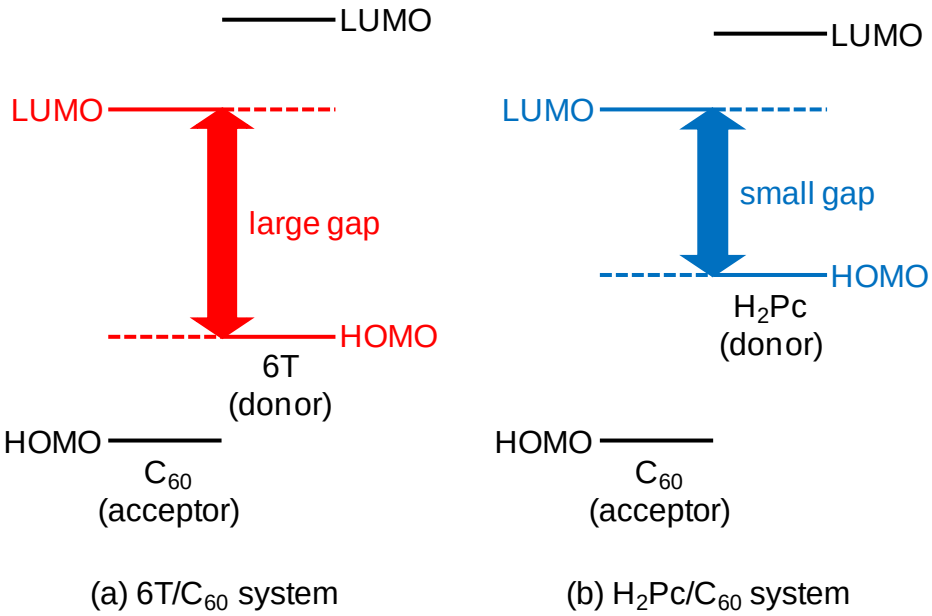

Fig. 1.3 Mechanism for the generation of open-circuit voltage.

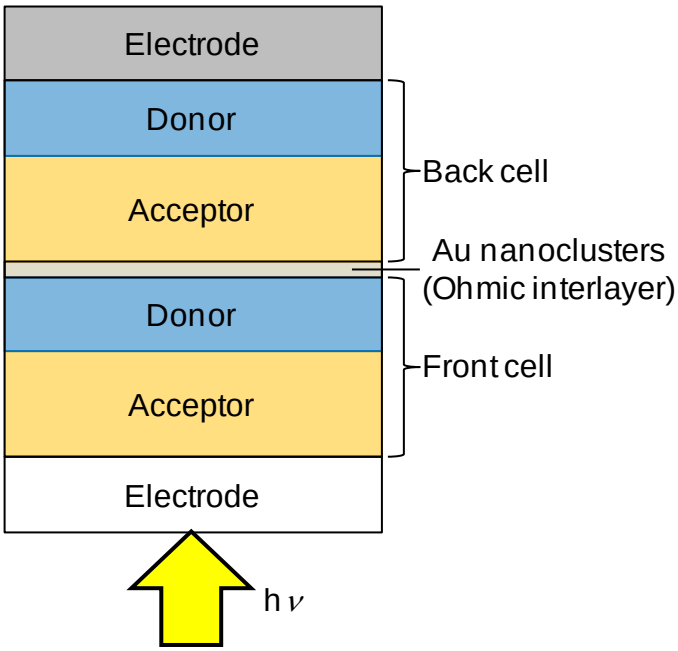

Fig. 1.4 Structure of a tandem organic photovoltaic cell incorporating Au nanoparticles as an ohmic interlayer.

Tandem cell formation is an effective method for doubling the V_{oc} value. In 1990, Hiramoto et al. proposed a tandem cell incorporating Au nanoparticles connecting two *pn*-heterojunction cells (**Fig. 1.4**).[32] Since then, other materials such as metal clusters,[33-37] metal oxides,[38-40] and organic materials[41] have been used for the ohmic interlayers. Currently, Timmreck et al. have reported on ohmic interlayers consisting of doped transparent organic semiconductors.[42-44]

1.4. Donor/Acceptor Sensitization

External quantum efficiency (EQE) is one important parameter for evaluating the performance of solar cells. EQE is expressed as the ratio of the number of electrons produced by photo irradiation to the number of photons irradiated to the cell. The EQE of an organic solar cell can be represented by **Eq. (1.1)**.

$$\mathrm{EQE} = \eta_{\alpha} \times \eta_{\mathrm{ed}} \times \eta_{\mathrm{ct}} \times \eta_{\mathrm{cc}} \quad (1.1)$$

η_{α}: the efficiency of absorption (causing the formation of an exciton, which is a bound state consisting of a hole and an electron).

η_{ed}: the efficiency of exciton diffusion to sites for dissociation.

η_{ct}: the probability of dissociation of excitons to free holes and electrons via charge transfer processes.

η_{cc}: the efficiency of carrier transport to the contacts, resulting in carrier collection by the corresponding electrode.

The magnitude of the exciton binding energy (*F*) obeys Coulomb's Law (**Eq. (1.2)**).

$$F = \frac{1}{4\pi\varepsilon\varepsilon_0}\frac{q_1 q_2}{r^2} \quad (1.2)$$

This equation consists of a specific dielectric constant (ε), the dielectric constant of a vacuum (ε_0), the magnitudes of the charges (q_1 and q_2), and the distance between the charges (r). In the case of materials with large ε values, the exciton binding energy is small. In the case of inorganic solar cells, since the ε values of Si and GaAs are as high as 12 and 13, respectively, excitons formed under photo irradiation have significantly larger radii; much larger than 10 nm. Thus, the excitons can be easily dissociated to free holes and electrons by the application of heat at room temperature, and a photocurrent is generated immediately.

On the other hand, organic solar cells have a problem in terms of exciton dissociation. Since the ε values of organic semiconductors are as low as 4,[45,46] the radii of any photo-induced excitons are around 1 nm. The exciton, in which a hole and an electron interact strongly with each other, is localized at an independent molecule (Frenkel exciton) (**Fig. 1.5(a)**). Thus, for single molecular films, the excitons are rarely dissociated and are almost immediately deactivated. As a result, η_{ct} is extremely low and photocurrents as low as 0.1 mA cm^{-2} are generated in cells consisting of single molecular films.[5,6,10,11]

On the other hand, for a combination of donors (D) and acceptors (A) consisting of two kinds of organic semiconductors that have different HOMO-LUMO levels from each other, the deactivation of excitons is avoided due to the formation of 'charge-transfer' (CT) excitons (**Fig. 1.5(b)**). Namely, the excitation of the acceptor is immediately followed by charge-transfer between the HOMO of the donor and the HOMO of the acceptor. The CT exciton can be easily dissociated into a free hole and an electron. Thus, η_{ct} becomes considerably higher than the equivalent values in

single molecular films. As a result, photocurrents of significant magnitude are generated in cells that make use of D/A sensitization.

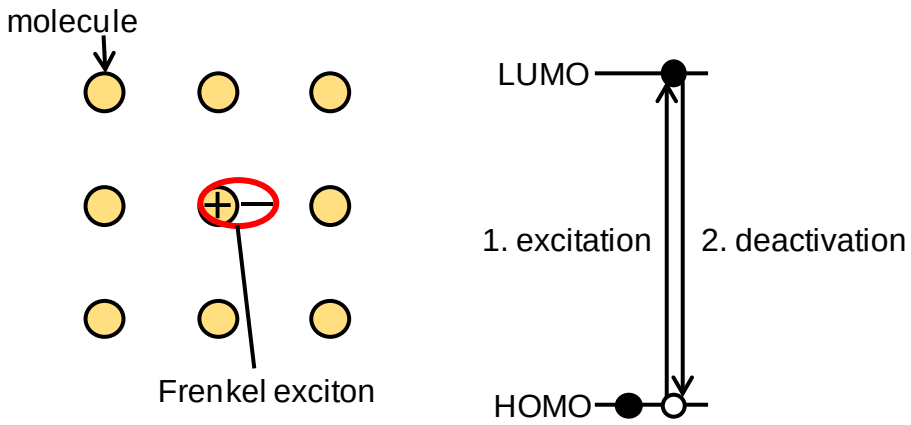

(a) single molecular system

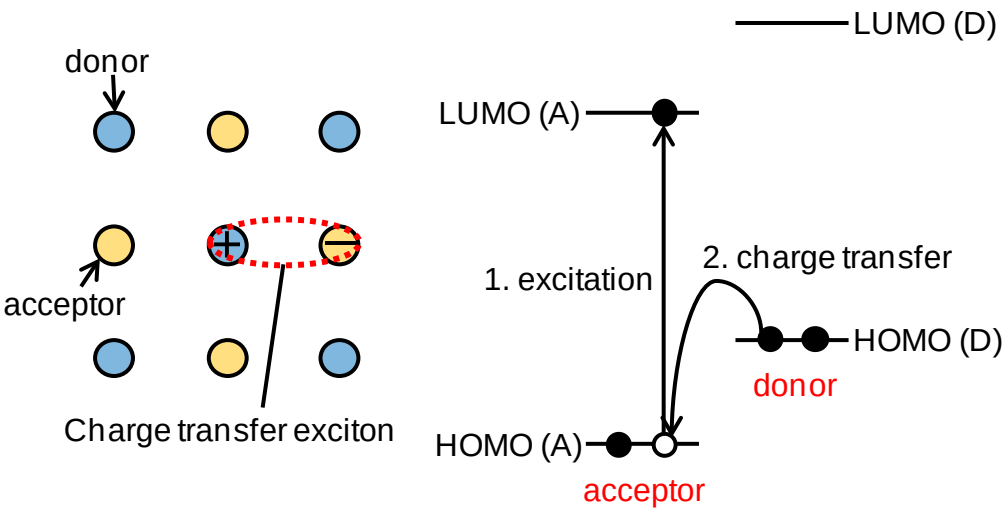

(b) Donor/acceptor system

Fig. 1.5 Mechanisms of carrier generation in organic photovoltaic cells.

1.5. Impurity Doping

Doping-based control of the energy structure is a matter of great importance for organic solar cells.[47] Impurity doping, which enables control of the conduction type and the reduction of the bulk resistance in a semiconductor, induces charge-transfer between a semiconductor and a dopant. When there is an overlap in energy regions between the band-gaps of two organic semiconductors, photoinduced CT (D/A sensitization) occurs (**Fig. 1.6(a)**) (see also **section 1.4**). On the other hand, in cases where there is no overlap in the band-gaps, doping-induced CT can be caused (**Fig. 1.6(b)**). For *p*-type doping, an acceptor dopant withdraws an electron from the valence band (VB) of a semiconductor, that is, the dopant injects a hole into the VB of the semiconductor. For *n*-type doping, a donor dopant injects an electron into conduction band (CB) of the semiconductor. Thus, the characteristics of organic semiconductors can be controlled by impurity doping.

In the case of organic solar cells, doping has mainly been applied for making ohmic contacts at hetero interfaces.[48,49] Leo et al. proposed the use of organic dopants for the formation of ohmic metal/organic contacts.[50,51] 2,3,5,6-Tetrafluoro-7,7,8,8-tetracyanoquinodimethan (F_4-TCNQ) and acridine orange base (AOB) were used as acceptor and donor dopants, respectively (**Fig. 1.7**). Currently, heavily-doped organic *pn*-heterojunctions have been used for the ohmic interlayers of tandem organic photovoltaic cells.[42-44]

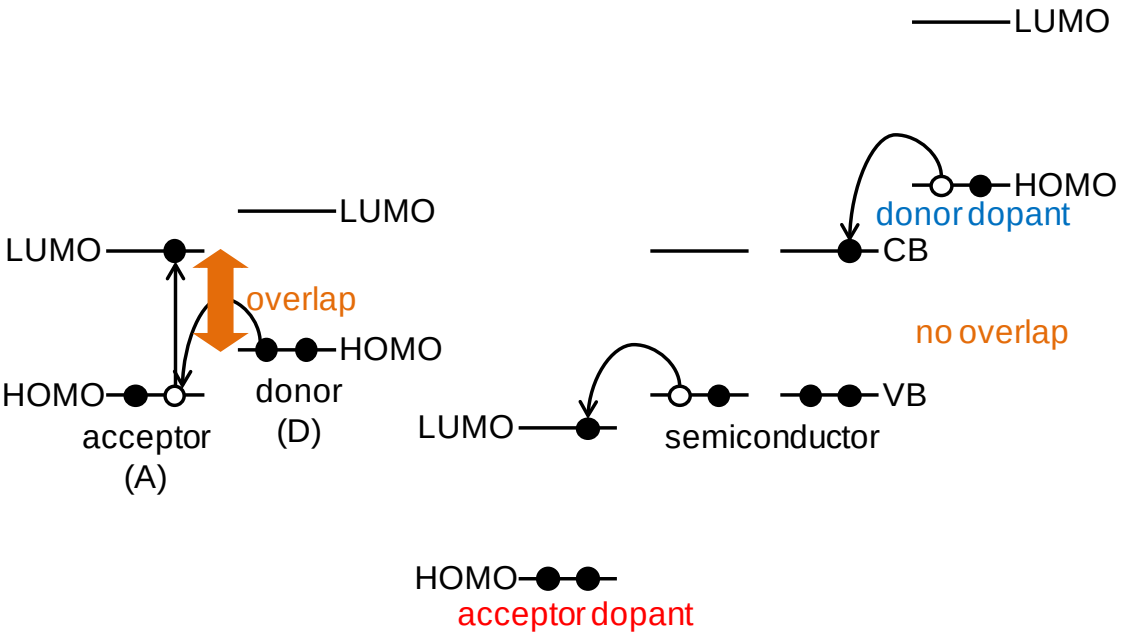

(a) Photoinduced charge transfer (D/A sensitization)

(b) Doping-induced charge transfer

Fig. 1.6 Difference in charge-transfer mechanisms between D/A sensitization and doping.

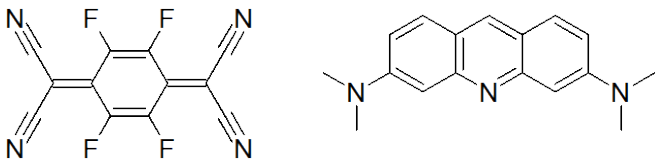

F_4-TCNQ (*p*-type dopant)

AOB (*n*-type dopant)

Fig. 1.7 Dopants for organic semiconductors.

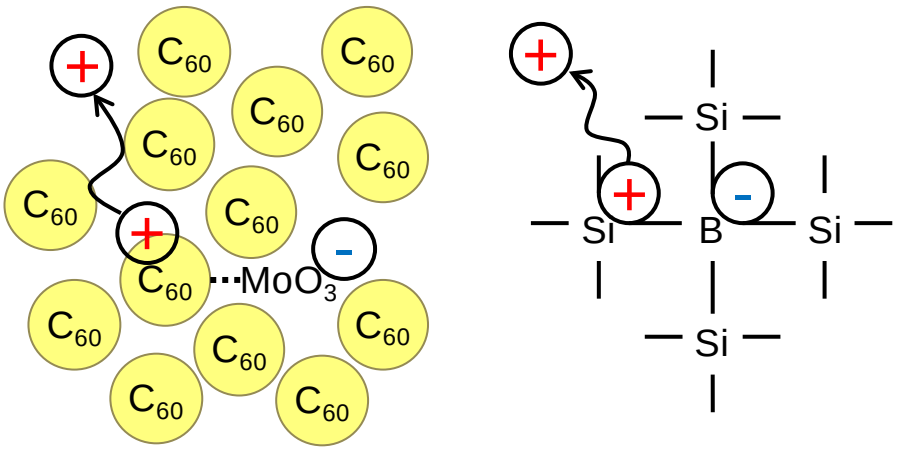

MoO_3 doping into C_{60} B doping into Si

(a) *p*-type doping

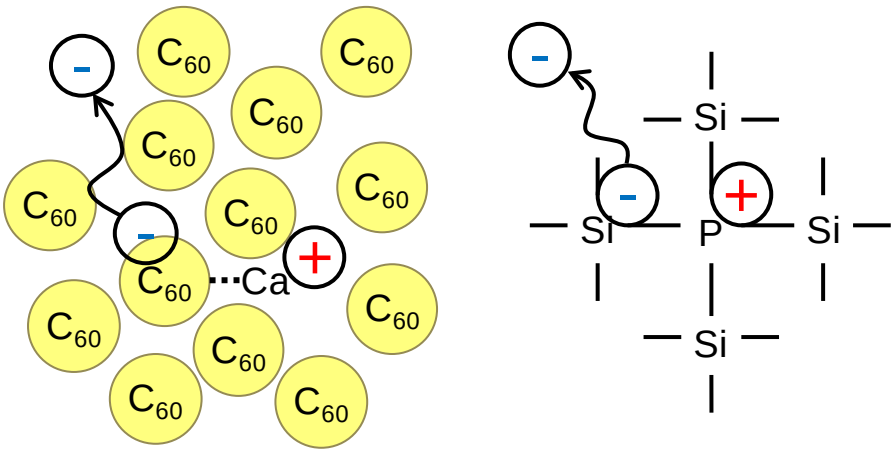

Ca doping into C_{60} P doping into Si

(b) *n*-type doping

Fig. 1.8 Mechanism of doping into single C_{60} films.

On the other hand, the design of the energy structures such as *pn*, *pin*, and p^+n^+-homojunctions, in organic semiconductors is also a key issue, just as it is in Si and GaAs devices.[47,52] In early works, the formation of *pn*-homojunctions in perylene

derivatives[53] and in zinc phthalocyanine[54] was demonstrated. Recently, Kubo et al. reported *pn*-control and *pn*-homojunction formation in single C_{60} films by doping with molybdenum oxide (MoO_3) and Ca.[5,6] For MoO_3-doped C_{60}, since the work function of MoO_3 (6.7 eV) is more positive than the VB of C_{60} (6.4 eV), MoO_3 accepts electrons from C_{60} (**Fig. 1.8(a)**) and forms charge-transfer complexes, i.e., C_{60}^{+}--- MoO_3^{-}. Here, the negative charge can be regarded as a spatially-fixed ionized MoO_3 acceptor. The positive charge on C_{60}^{+} can be liberated by thermal energy at room temperature and acts as a free hole in the VB of C_{60}, making it *p*-type. This process is similar to P doping into Si. On the other hand, in the case of Ca-doped C_{60}, since the work function of Ca (1.9 eV) is more negative than the CB of C_{60} (4.0 eV), Ca donates electrons to the C_{60} (**Fig. 1.8(b)**) and forms charge-transfer complexes, i.e., C_{60}^{-}--- Ca^{+}. The negative charge liberated from C_{60}^{-} makes the C_{60} *n*-type. This process is similar to B doping into Si.

By using MoO_3 and Ca doping, *pn*-homojunctions were fabricated in single C_{60} films (**Fig. 1.9**). Since there is a significant energy difference in the Fermi level positions between the MoO_3-doped *p*-C_{60} (5.9 eV) and Ca-doped *n*-C_{60} (4.5 eV) regions (**Fig. 1.9(a)**), a built-in potential can be created by forming a contact between MoO_3 and Ca doped C_{60} films (**Fig. 1.9(b)**). A photoactive depletion layer is formed at the MoO_3/Ca doped interface.

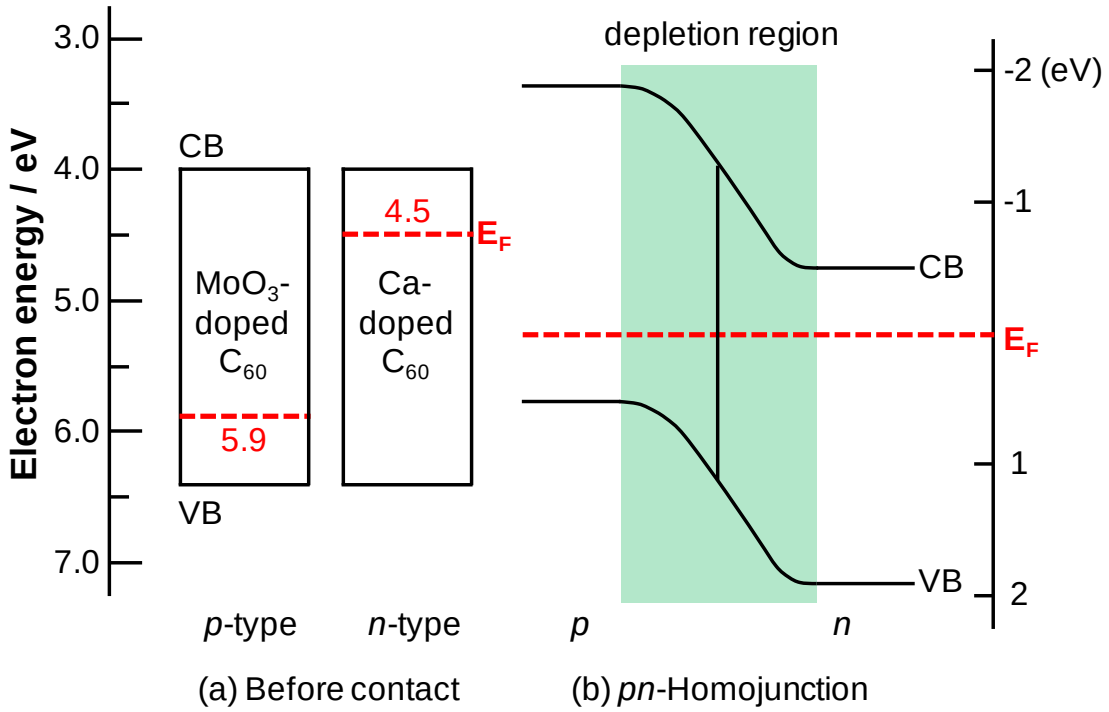

Fig. 1.9 Energy band diagram of C_{60} films doped with MoO_3 and Ca.

1.6. Aim of this Thesis

Currently, most organic solar cells incorporate co-deposited films that consist of two kinds of organic semiconductors in order to extend the active regions for improved photocurrent generation. As in the case of inorganic solar cells, precise *pn*-control and the formation of *pn*, *pin*, and p^+n^+ homojunctions have been applied directly to photoactive semiconductors in order to design more efficient cells.[47,52,55-57] However, there has been no attempt to control the energy structure of photoactive co-deposited films by doping. The author believes that the formation of *pn*-homojunctions directly in the bulk of co-deposited films has a high potential to enhance the efficiency of cells for the following reasons. (i) A built-in electric field can be constructed directly in the co-deposited region where the generation and

transport of photocarriers occurs (**Fig. 1.10**). (ii) Reducing the bulk resistance of co-deposited films by doping can enable the growth of co-deposited films that are sufficiently thick (e.g. 1 μm) to absorb the whole of the incident solar light and to convert it to a photocurrent. Based on these considerations, the author attempted to develop a doping technique for a co-deposited film that could be regarded as a single semiconductor.

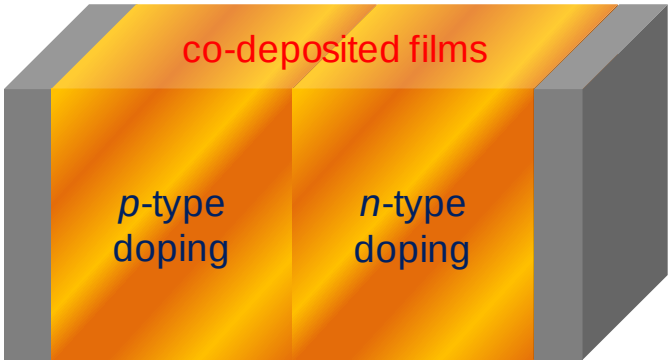

Fig. 1.10 Conceptual diagram of doping into a photovoltaic organic co-deposited film.

1.7. References

1) M. A. Green, K. Emery, Y. Hishikawa, W. Warta, and E. D. Dunlop, *Prog. Photovolt*: *Res. Appl*., **20**, 606 (2012).
2) J. Sakai, T. Taima, and K. Saito, *Org. Electron*., **9**, 582 (2008).
3) J. Sakai, T. Taima, T. Yamanari, and K. Saito, *Sol. Energy Mater. Sol. Cells*, **93**, 1149 (2009).
4) S. Tokito, K. Noda, and Y. Taga, *J. Phys. D*: *Appl. Phys*., **29**, 2750 (1996).
5) M. Kubo, T. Kaji, K. Iketaki, and M. Hiramoto, *Appl. Phys. Lett*., 98, 073311 (2011).
6) M. Kubo, T. Kaji, and M. Hiramoto, *AIP Advances*, **1**, 032177 (2011).
7) H.–H. Liao, L.–M. Chen, Z. Xu, G. Li, and Y. Yang, *Appl. Phys. Lett.*, **92** 173303 (2008).
8) S. Hamwi, T. Riedl, W. Kowalsky, *Appl. Phys. Lett*., **99**, 053301 (2011).
9) D. R. Kearns and M. Calvin, *J. Chem. Phys.*, **29**, 950 (1958).
10) G. A. Chamberlain, *Solar Cells*, **8**, 47 (1983).
11) H. Spanggaard and F. C. Krebs, *Sol. Energy Mater. Sol. Cells*, **83**, 125 (2004).
12) C. W. Tang, *Appl. Phys. Lett*., **48**, 183 (1986).
13) P. Peumans, A. Yakimov, and S. R. Forrest, *J. Appl. Phys*., **93**, 3693 (2003).
14) M. Hiramoto, H. Fujiwara, and M. Yokoyama, *Appl. Phys.* Lett., **58**, 1062 (1991).
15) M. Hiramoto, H. Fujiwara, and M. Yokoyama, *J. Appl. Phys.*, **72**, 3781 (1992).
16) P. Peumans, S. Uchida, and S. R. Forrest, *Nature*, **425**, 158 (2003).
17) T. Taima, M. Chikamatsu, Y. Yoshida, K. Saito, and K. Yase, *Appl. Phys. Lett*., **85**, 6412 (2004).
18) J. Xue, B. P. Rand, S. Uchida, and, S. R. Forrest, *Adv. Mater.*, **17**, 66 (2005).

19) K. Suemori, T. Miyata, M. Yokoyama, and M. Hiramoto, *Appl. Phys. Lett.*, **86**, 063509 (2005).

20) T. Kaji, M. Zhang, S. Nakao, K. Iketaki, K. Yokoyama, C. W. Tang, and M. Hiramoto, *Adv. Mater.*, **23**, 3320 (2011).

21) Y. Zhou, T. Taima, T. Miyadera, T. Yamanari, M. Kitamura, K. Nakatsu, and Y. Yoshida, *Appl. Phys. Lett.*, **100**, 233302 (2012).

22) D. Wynands, M. Levichkova, K. Leo, C. Uhrich, G. Schwartz, D. Hildebrandt, M. Pfeiffer, and M. Riede, *Appl. Phys. Lett.*, **97**, 073503 (2010).

23) N.S. Sariciftci, D. Braun, C. Zhang, V.I. Srdanov, A.J. Heeger, G. Stucky, F. Wudl, *Appl. Phys. Lett.*, **62** 585 (1993).

24) M. Hiramoto, K. Kitada, K. Iketaki, and T. Kaji, *Appl. Phys. Lett.*, **98**, 023302 (2011).

25) J. Meiss, F. Holzmueller, R. Gresser, K. Leo, and M. Riede, *Appl. Phys. Lett.*, **99**, 193307 (2011).

26) W. Chen, X. Qiao, J. Yang, B. Yu, and D. Yan, *Appl. Phys. Lett.*, **100**, 133302 (2012).

27) K. Schulze, C. Uhrich, R. Schuppel, K. Leo, M. Pfeiffer, E. Brier, E. Reinold, and P. Bauerle, *Adv. Mater.*, **18**, 2872 (2006).

28) D. Wynands, M. Levichkova, M. Riede, M. Pfeiffer, P. Baeuerle, R. Rentenberger, P. Denner, and K. Leo, *J. Appl. Phys.*, **107**, 014517 (2010).

29) V. Steinmann, N. M. Kronenberg, M. R. Lenze, S. M. Graf, D. Hertel, H. Burckstummer, F. Wurthner, and K. Meerholz, *Appl. Phys. Lett.*, **99**, 193306 (2011).

30) T. Taima, J. Sakai, T. Yamanari and K. Saito, *Jpn. J. Appl. Phys.*, **45**, 995 (2006).

31) M. Zhang , H. Wang , H. Tian , Y. Geng , and C. W. Tang, *Adv. Mater.*, **23**, 4960

(2011).

32) M. Hiramoto, M. Suezaki, and M. Yokoyama, *Chem. Lett.*, **19**, 327 (1990).

33) A. Yakimov and S. R. Forrest, *Appl. Phys. Lett.*, **80**, 1667 (2002).

34) J. Xue, S. Uchida, B. P. Rand, and S. R. Forrest, *Appl. Phys. Lett.*, **85**, 5757 (2004).

35) T. Ameri, G. Dennler, C. Lungenschmied and C. J. Brabec, *Energy Environ. Sci.*, **2**, 347 (2009).

36) M. Zhang, H. Wang, C.W. Tang, *Org. Electron.*, **13**, 249 (2012).

37) Y. Zou, Z. Deng, W. J. Potscavage, M. Hirade, Y. Zheng, and C. Adachi, *Appl. Phys. Lett.*, **100**, 243302 (2012).

38) J. Gilot, M. M. Wienk, and R. A. J. Janssen, *Appl. Phys. Lett.*, **90**, 143512 (2007).

39) L. Dou, J. You, J. Yang, C.-C. Chen, Y. He, S. Murase, T. Moriarty, K. Emery, G. Li, and Y. Yang, *Nature Photon.*, **6**, 180 (2012).

40) G. Li, R. Zhu, and Y. Yang, *Nature Photon.*, **6**, 153 (2012).

41) B. Yu, F. Zhu, H. Wang, G. Li, and D. Yan, *J. Appl. Phys.*, **104**, 114503 (2008).

42) R. Timmreck, S. Olthof, K. Leo, and M. K. Riede, *J. Appl. Phys.*, **108**, 033108 (2010).

43) R. Schueppel, R. Timmreck, N. Allinger, T. Mueller, M. Furno, C. Uhrich, K. Leo, and M. Riede, *J. Appl. Phys.*, **107**, 044503 (2010).

44) M. Riede, C. Uhrich, J.Widmer, R. Timmreck, D. Wynands, G. Schwartz, W.-M. Gnehr, D. Hildebrandt, A. Weiss, J. Hwang, S. Sundarraj, P. Erk, M. Pfeiffer, and Karl Leo, *Adv. Funct. Mater.*, **21**, 3019 (2011).

45) A. F. Hebard, R. C. Hadon, R. M. Fleming, and A. R. Kortan, *Appl. Phys. Lett.*, **59**, 2109 (1991).

46) M. A. Abkowitz and A. I. Lakatos, *J. Chem. Phys.* **57**, 5033 (1972).

47) W. E. Spear and P. E. Lecomber, *Solid State Commun*., **17**, 1193 (1975).

48) J. C. deMello, N. Tessler, S. C. Graham, and R. H. Friend, *Phys*. *Rev*. *B*, **57**, 12951 (1998).

49) M. Hiramoto, A. Tomioka, K. Suemori, and M. Yokoyama, *Appl*. *Phys*. *Lett*., **85**, 1852 (2004).

50) K. Walzer, B. Maennig, M. Pfeiffer, and K. Leo, *Chem*. *Rev*., **107**, 1233 (2007).

51) C. Falkenberg, C. Uhrich, S. Olthof, B. Maennig, M. K. Riede, and K. Leo, *J*. *Appl*. *Phys*., **104**, 034506 (2008).

52) R. P. Leon, S. G. Bailey, G. A. Mazaris, and W. D. Williams, *Appl*. *Phys*. *Lett*., **49**, 945 (1986).

53) M. Hiramoto, K. Ihara, and M. Yokoyama, *Jpn*. *J*. *Appl*. *Phys*., **34**, 3803 (1995).

54) K. Harada, A. G. Werner, M. Pfeiffer, C. J. Bloom, C. M. Elliott, and K. Leo, *Phys*. *Rev*. *Lett*., **94**, 036601 (2005).

55) M. Ilegems, B. Schwartz, L. A. Koszi, and R. C. Miller, *Appl*. *Phys*. *Lett*., **33**, 629 (1978).

56) Y. Hamakawa, H. Okamoto, and Y. Nitta, *Appl*. *Phys*. *Lett*., **35**, 187 (1979).

57) C. Amano, H. Sugiura, A. Yamomoto, and M. Yamaguchi, *Appl*. *Phys*. *Lett*., **51**, 1998 (1987).

Chapter 2:

Fundamental Equipment and Methods

2.1. Purification of Materials

Fullerene (C_{60}) (Frontier Carbon, nanom purple TL) and α-sexithiophene (6T) (Tokyo Chemical Industry) samples were purified by single-crystal sublimation[1,2] under flowing N_2 at 1 atm and 0.1 atm, respectively. The author used a custom-designed purification system (Epi Tech Inc.) equipped with a three-zone infrared heating furnace (Thermo Riko, GFB 460-3Z) (**Fig. 2.1**) and grew millimeter-scale crystals (**Fig. 2.2**). Bathocuproine (Dojindo Laboratories, sublimated), molybdenum oxide (MoO_3) (Alfa Aeser, 99.9995%) and cesium carbonate (Cs_2CO_3) (Sigma-Aldrich, 99.995%) were used without further purification. Ag (Nacalai Tesque, 99.99%) was used for the electrodes.

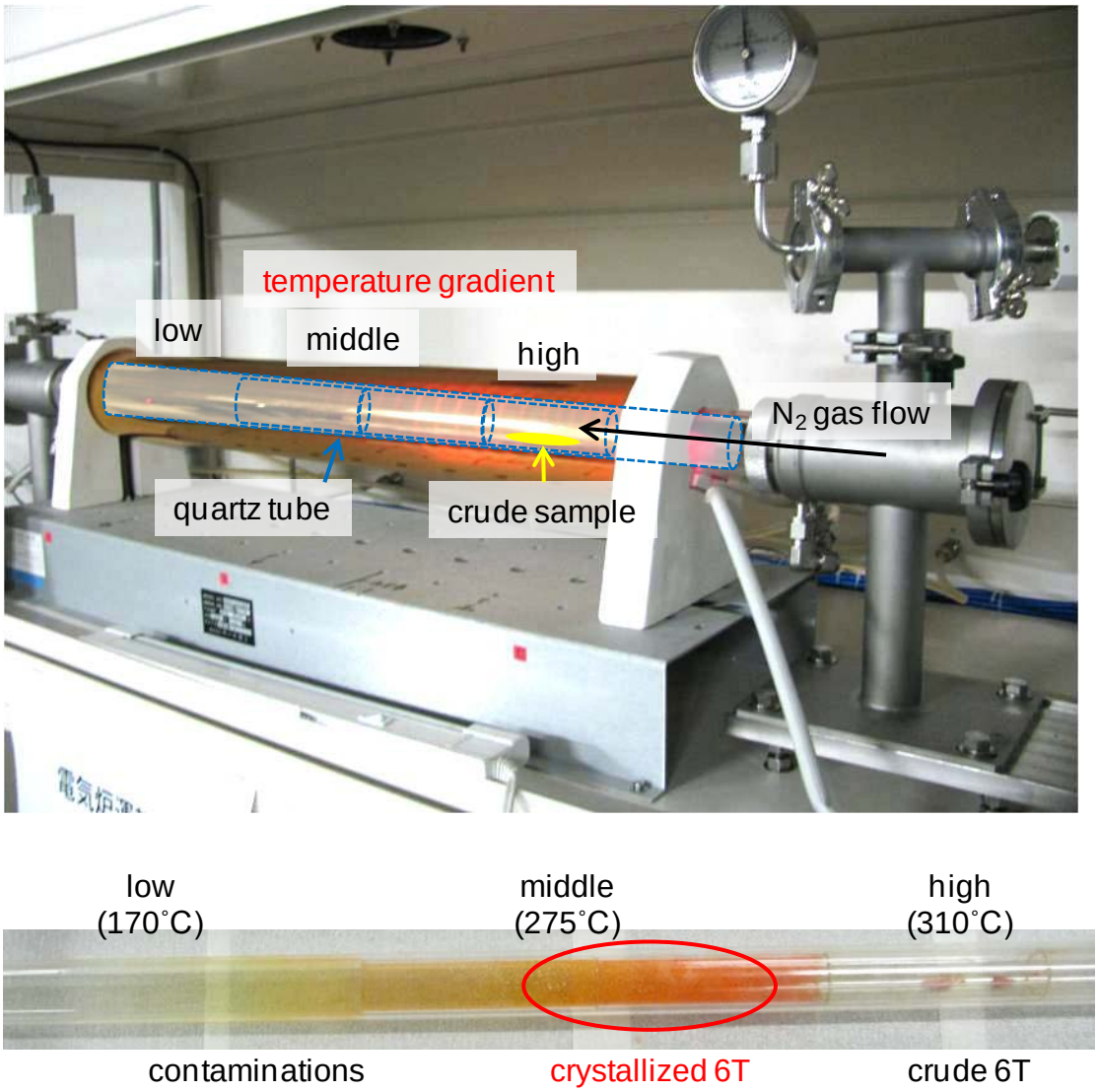

Fig. 2.1 Purification of a 6T sample using a single crystal sublimation system equipped with a three-zone heating furnace.

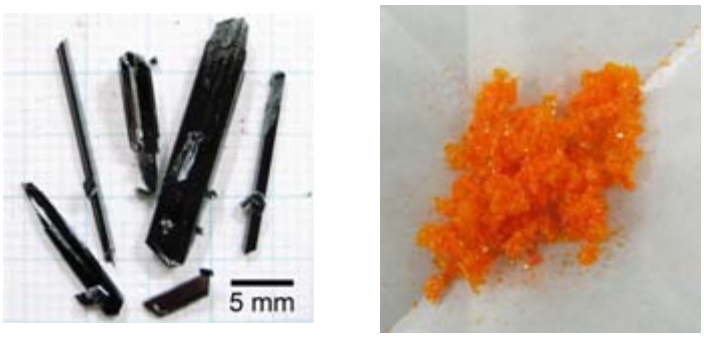

fullerene (C_{60}) α-sexithiophene (6T)

Fig. 2.2 Purified organic semiconductors.

2.2. Fabrication of Cells

A process chart of the cell fabrication is shown in **Fig. 2.3**. Indium tin oxide (ITO) coated glass substrates (Sanyo Vacuum Industries) (**Fig. 2.3 (a)**) were washed three times with water (10 min), methanol (10 min), and acetone (10 min), respectively in an ultrasonic bath. All of the films were deposited by vacuum evaporation onto ITO glass substrates at 10^{-4} Pa using an oil-free vacuum evaporator (Epi Tech Inc., ET300-6E-HK) (**Fig. 2.4**). The film thicknesses were monitored simultaneously with the deposition using quartz crystal microbalances (QCM). The film thicknesses monitored by the QCM were calibrated using a surface profilometer (Dektak) (**Fig. 2.5**). For fabricating a co-deposited film consisting of C_{60} and 6T (C_{60}:6T) (10:1) (**Fig. 2.3 (b)**), C_{60} and 6T were evaporated from two different sources at deposition rates of 0.2 nm s^{-1} and 0.02 nm s^{-1}, respectively. The cell area onto which the Ag electrode was deposited was defined using a metal mask with an aperture of 0.06 cm^{-2} (**Fig. 2.3 (c)**).

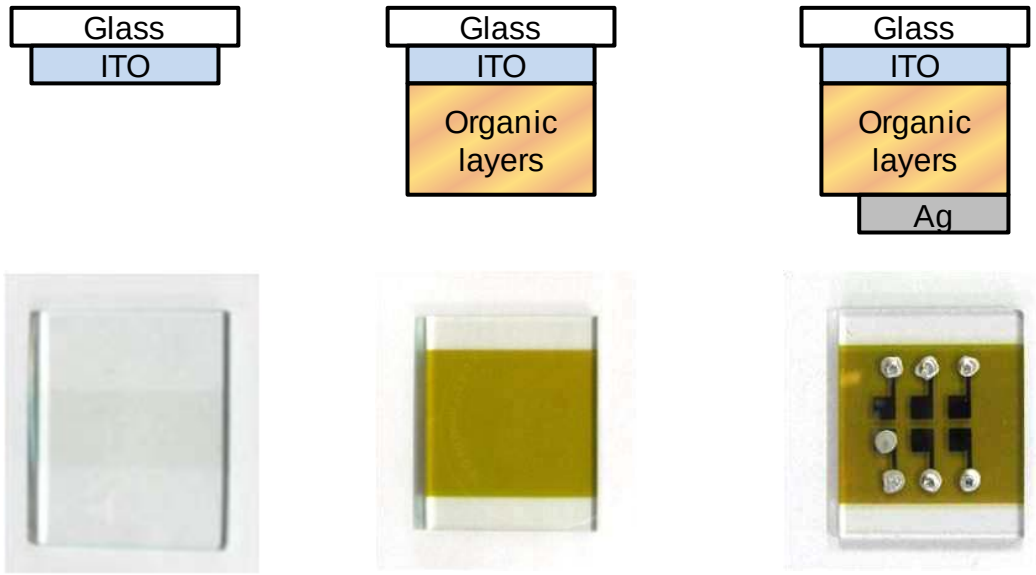

(a) ITO glass substrate (b) Deposition of organic layers (c) Deposition of Ag electrode

Fig. 2.3 Process chart of the cell fabrication.

Fig. 2.4 Vacuum evaporator.

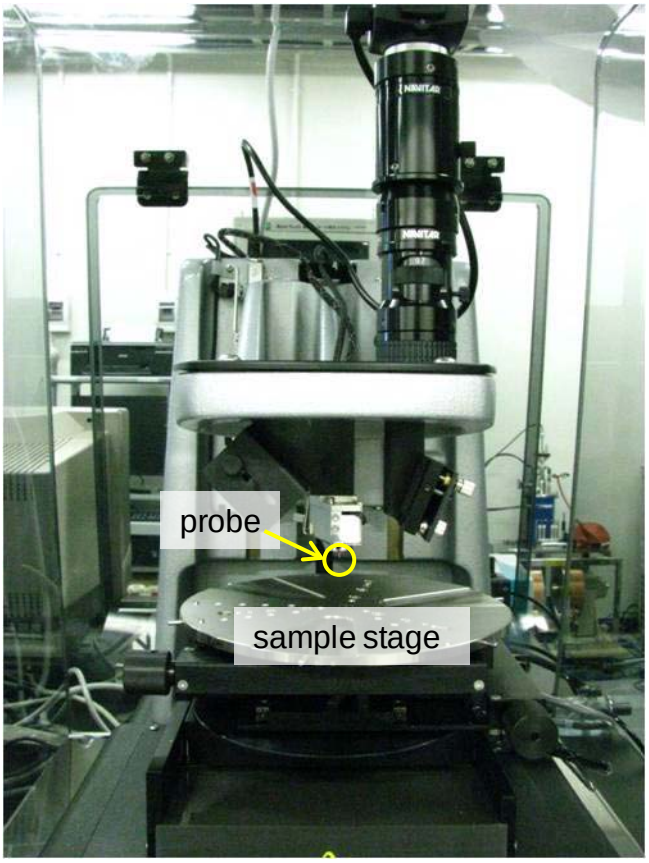

Fig. 2.5 Surface profilometer (Dektak).

2.3. 'Three Component Co-evaporation' Technique

Doping into a co-deposited film was performed using a 'three component co-evaporation' technique, in which three different evaporation sources were used (**Fig. 2.6**). Precise monitoring of the deposition rate of the dopant at 1 x 10^{-5} nm s^{-1} was achieved using quartz crystal microbalances (QCM) equipped with a computer monitoring system (ULVAC, Depoview), which allowed us to dope with Cs_2CO_3 as low as 40 ppm by volume concentration (**Fig. 2.7**). The distances from the Cs_2CO_3 source to the QCM and to the substrate were 9 and 18 cm, respectively. The tooling factor as determined by the surface profilometer was 0.25. The relationship between the total-thickness signal from the QCM vs. time was monitored using a PC display. For 40 ppm Cs_2CO_3, there was a very slow cyclic fluctuation (frequency: ~300 s, amplitude: ~0.05 nm) caused by temperature variations in the coolant water for the QCM. A reproducible increase in the baseline of 0.04 nm, which was only noted during Cs_2CO_3 evaporation over a prolonged timescale of 3600 seconds, was observed (1 x 10^{-5} nm s^{-1}).

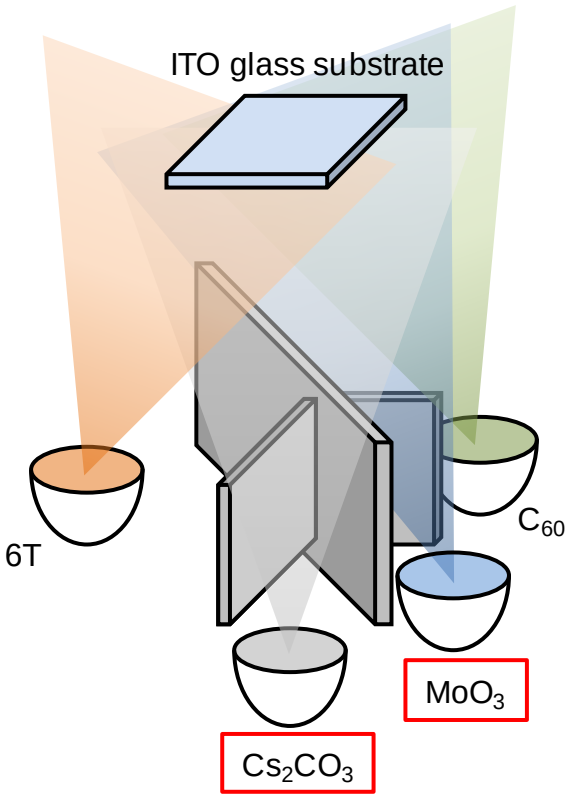

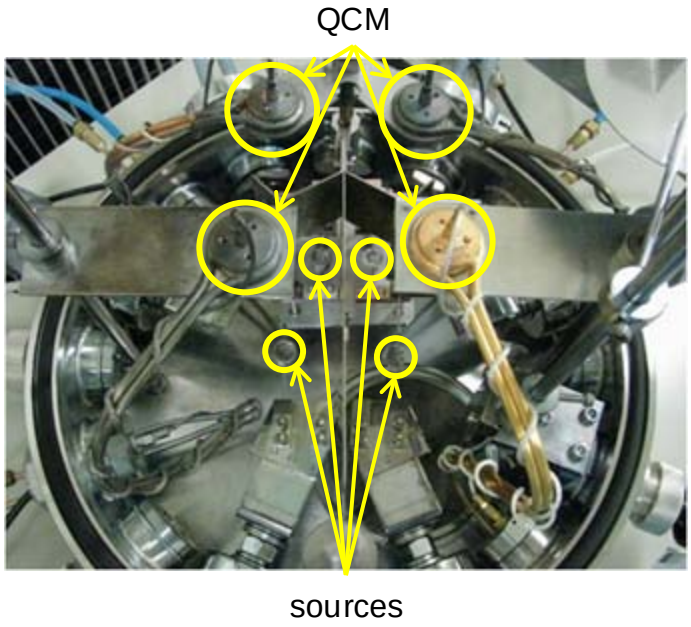

Fig. 2.6 Equipment for a ‘three component co-evaporation’ technique.

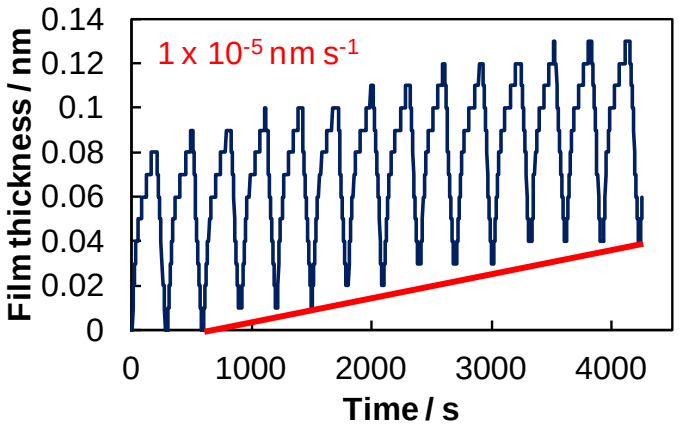

Fig. 2.7 Precise monitoring of deposition rate using a computer monitoring system.

2.4. Measurements of Photovoltaic Properties

The photovoltaic properties of the cells were measured by setting the cells into a sample container equipped with a quartz glass window (Epi Tech Inc.) (**Fig. 2.8(a)**). The container was evacuated to 10^{-3} Pa, and the current-voltage (J-V) characteristics and action spectra were measured by irradiating with simulated solar light (Yamashita Denso, YSS-50A) (AM1.5, 100 mW cm^{-2}) (**Fig. 2.9**), and with monochromatic light from a Xe-lamp (Shimadzu, SPG-3ST) through a monochromator (**Fig. 2.10**), respectively. The photo-irradiated cell area was precisely defined using a metal mask with an aperture of 0.04 cm^{-2} (**Fig. 2.8(b)**).

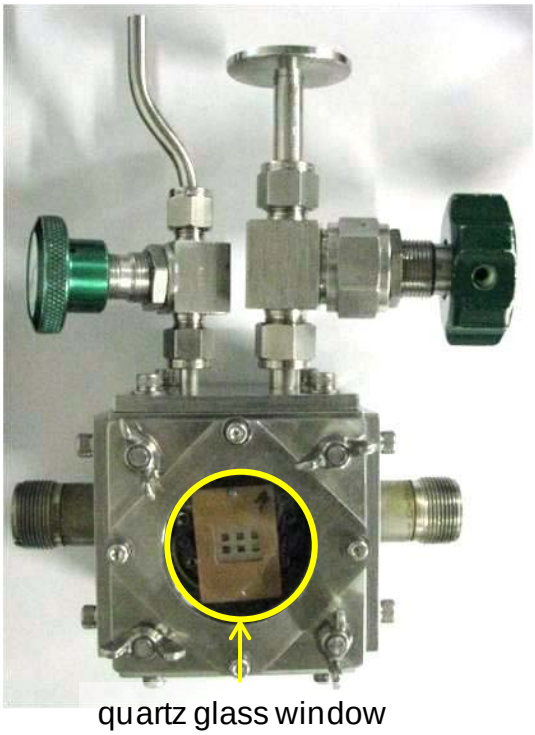

(a) Sample container with a quartz glass window.

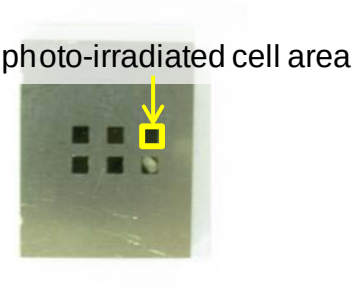

(b) Metal mask with an aperture of 0.04 cm^{-2}.

Fig. 2.8 Instruments for the measurement of the photovoltaic properties of the cells.

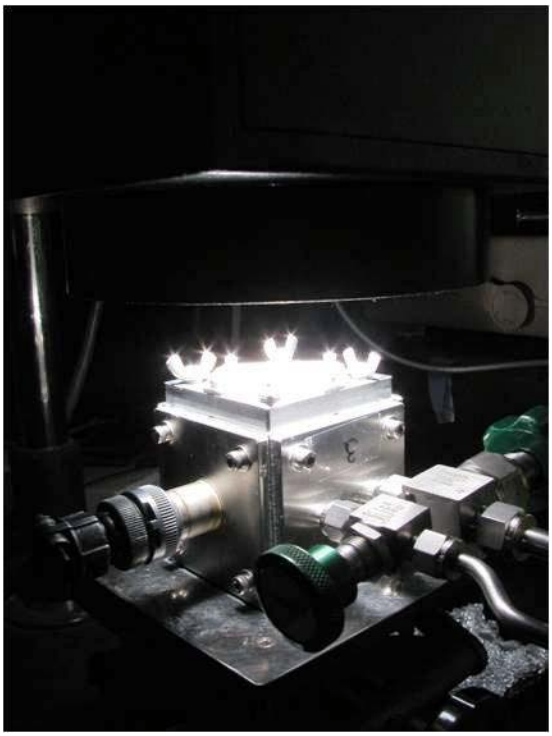

Fig. 2.9 Irradiation of simulated solar light to the cell.

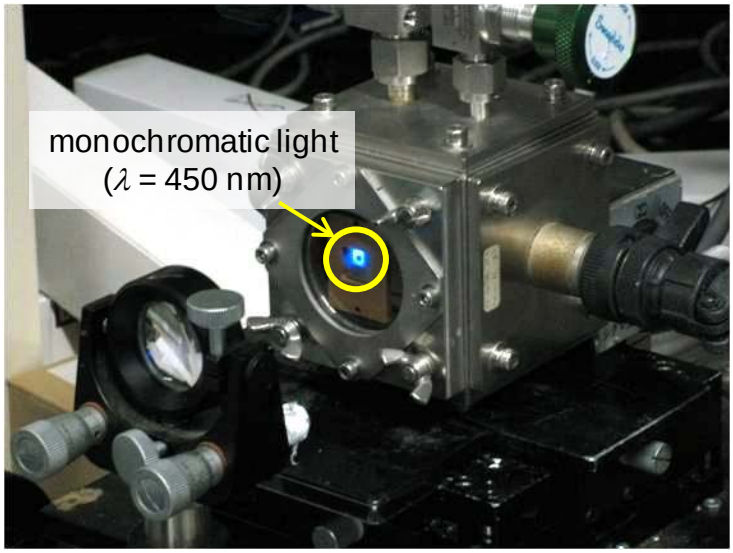

Fig. 2.10 Irradiation of monochromatic light to the cell.

Fig. 2.11 shows the typical current-voltage (*J*-*V*) characteristics in the dark and under irradiation with simulated solar light. Various parameters, including the short-circuit photocurrent density (J_{sc}), the open-circuit voltage (V_{oc}), and the values of current and voltage (J_m and V_m) for the maximum power output (P_{out}) are also shown. The power conversion efficiency (η_p) is calculated using **Eq. (2.1)**.

$$\eta_P = \frac{P_{out}}{P_{in}} = \frac{J_{sc} \times V_{oc} \times FF}{P_{in}} \quad (2.1)$$

Here, P_{in} is the incident light intensity. Typically, AM 1.5G (100 mW cm^{-2}) is used for P_{in}. The fill factor (FF) is calculated as **Eq. (2.2)**.

$$FF = \frac{P_{out}}{J_{sc} \times V_{oc}} = \frac{J_m \times V_m}{J_{sc} \times V_{oc}} \quad (2.2)$$

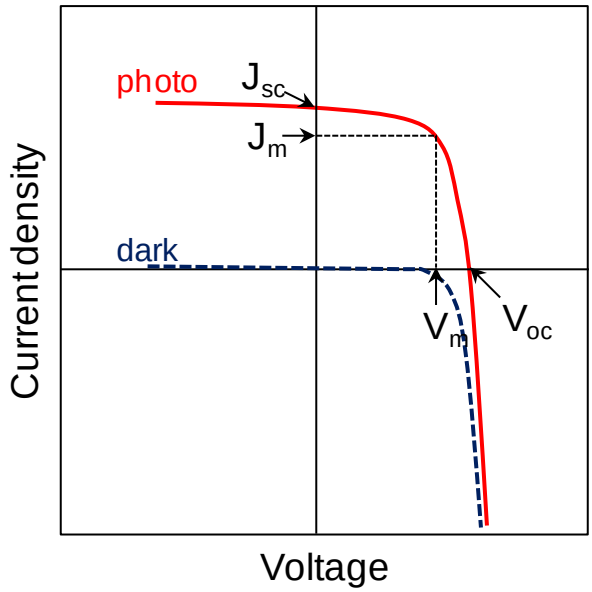

Fig. 2.11 Typical current-voltage (J-V) characteristics of a cell.

2.5. Kelvin Probe Measurements

The Fermi levels (E_F) of the organic films were measured using a Kelvin vibrating capacitor apparatus (Riken-Keiki, FAC-1) (**Fig. 2.12**).[3,4] Both the vacuum evaporator and the Kelvin probe were built into a glove-box (Miwa, DBO-1.5) (**Fig. 2.13(a)**) that was purged with N_2 gas. The concentrations of H_2O and O_2 were kept below 0.5 and 0.2 ppm, respectively. Thus, during the film deposition and E_F measurements, the films were not exposed to air at any time.

Fig. 2.12 Glove box with a built-in vacuum evaporator.

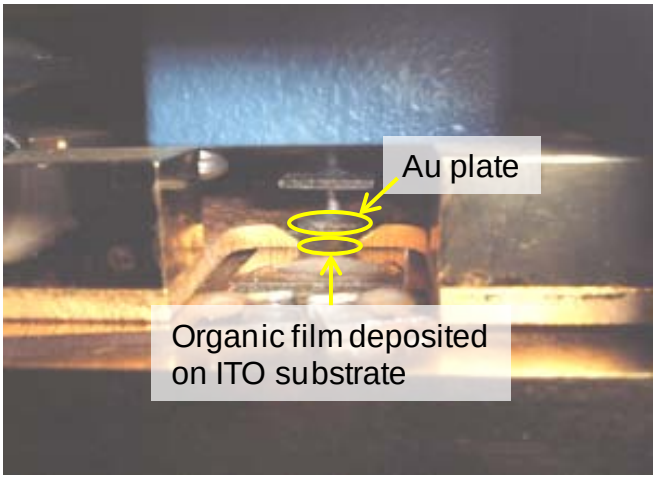

Fig. 2.13 (a) Kelvin vibrating capacitor apparatus (Kelvin probe).

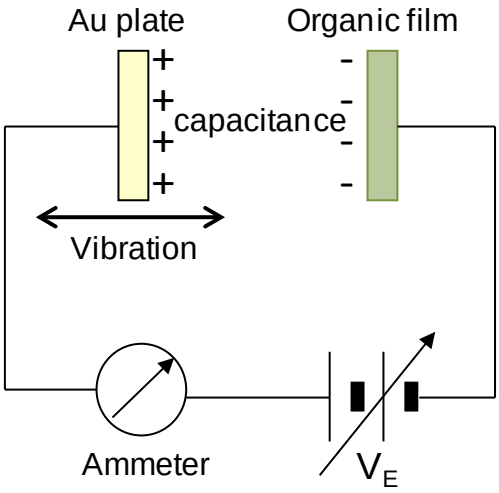

(b) Schematic diagram of the Kelvin probe method.

Fig. 2.13 (b) shows a schematic diagram of the Kelvin probe method. When a capacitor with a capacitance (C) is formed by an Au plate and an organic film that have work functions of Φ_{Au} and Φ_S, respectively, a charge (Q) (**Eq. 2.3**) is induced on the conductive plates due to the difference in contact potentials ($\Phi_{Au} - \Phi_S$).

$$Q = C(\Phi_S - \Phi_{Au}) \qquad (2.3)$$

When the capacitance is varied (ΔC) by vibrating the Au plate, the charge also varies

(**Eq. 2.4**) and an alternating current is generated.

$$\Delta Q = \Delta C(\Phi_S - \Phi_{Au}) \quad (2.4)$$

Here, ΔQ and ΔC are the charge difference and the capacitance difference, respectively. Moreover, in the case of applying an external voltage (V_E) to the capacitor, the charge difference ($\Delta Q'$) is represented by **Eq. 2.5**.

$$\Delta Q' = \Delta C(\Phi_S - \Phi_{Au} + V_E) \quad (2.5)$$

By applying V_E to the offset $\Delta Q'$, Φ_S can be determined by **Eq.2.6**.

$$\Phi_S = \Phi_{Au} - V_E(\Delta Q = 0) \quad (2.6)$$

Since the value of Φ_{Au} can be measured by x-ray photoelectron spectroscopy,[5] Φ_S is determined by the value of V_E ($\Delta Q' = 0$).

2.6. Energy Band Mapping of Doped Junctions

Energy-band mapping of the doped junctions was performed using a Kelvin probe.[6] **Fig. 2.14** shows the principle of mapping of a Schottky junction between ITO and a *p*-type doped organic film. When the organic film is placed in contact with an ITO substrate, the E_F of the film agrees with that of the ITO. As a result, the vacuum level (E_v) in the *p*-type film bends and a depletion layer appears at the ITO/organic layer interface (**Fig. 2.14**, red shaded region). In the depletion layer, the work function of the *p*-type film, which is defined by the energy difference between the Ev and E_F of the film (E_{FS}), shifts along with the band-bending. Therefore, when Kelvin probe measurements for different thicknesses of *p*-type films are employed, a shift in the work function, which represents the band-bending in the depletion layer, is observed. Thus, the energy band diagrams of *p*-type Schottky junctions can be depicted based on the

Kelvin probe measurements. This method can be also applied to energy mapping of homojunctions formed in organic films.

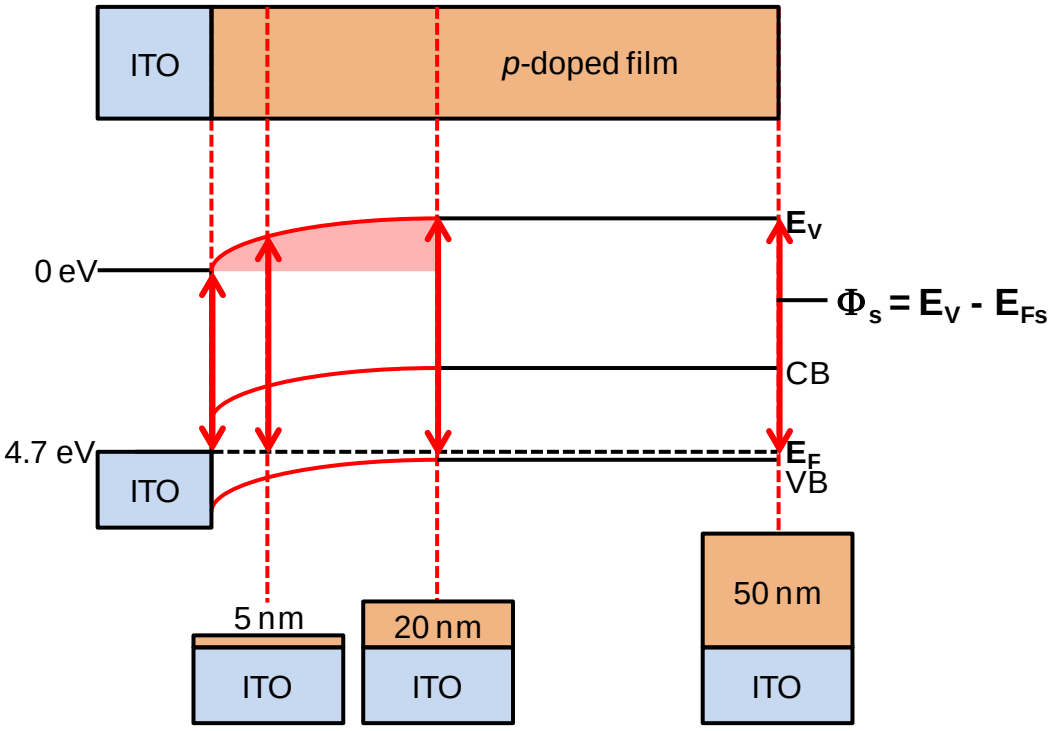

Fig. 2.14 Principle of energy-band mapping of doped junctions using a Kelvin probe. An example of a Schottky junction between ITO and a *p*-doped film is shown.

2.7. References

1) M. Hiramoto and K. Sakai, *Mol. Cryst. Liq. Cryst.*, **491**, 284 (2008).

2) R. A. Laudise, Ch. Kloc, P. G. Simpkins, and T. Siegrist, *J. Cyrstal Growth*, **187**, 449 (1998).

3) M. Hiramoto, K. Ihara, and M. Yokoyama, *Jpn. J. Appl. Phys.* 1, **34**, 3803 (1995).

4) M. Pfeiffer, K. Leo, and N. Karl, *J. Appl. Phys.*, **80**, 6880 (1996).

5) H. B. Michaelson, *J. Appl. Phys.*, **48**, 4729 (1977).

6) N. Hayashi, H. Ishii, Y. Ouchi, and K. Seki, *J. Appl. Phys.* **92**, 3784 (2002).

Chapter 3:

Function Control of *pn*-Homojunctions and the Formation of Tandem Photovoltaic Cells in Single Fullerene Films

"Tandem photovoltaic cells formed in single fullerene films by impurity doping", Norihiro Ishiyama, Masayuki Kubo, Toshihiko Kaji, and Masahiro Hiramoto, *Appl*. *Phys*. *Lett*., **101**, 233303 (2012).

Abstract

Tandem photovoltaic cells were formed in single fullerene films by doping with molybdenum oxide and cesium carbonate. A heavily doped n^+p^+-homojunction acted as an ohmic interlayer between the two *pn*-homojunction cells. The observed photovoltaic properties of the tandem cell were shown to be consistent with the energy band diagram mapped using a Kelvin probe.

3.1. Introduction

Controlling the *pn*-properties is fundamental to the construction of small-molecular-type organic photovoltaic cells[1-7] as well as inorganic ones.[8] Recently, the complete control of the *pn*-properties and the formation of a *pn*-homojunction in fullerene (C_{60}) [9,10] were reported. In addition, doubling the open-circuit photovoltage (V_{oc}) by use of an organic tandem cell has attracted the attention of many researchers. Organic tandem cell research started in 1990 when Au nanoparticles were incorporated to connect two unit cells together.[11] Since then, other materials such as metal clusters and metal oxides have been used for ohmic interlayers.[12-14] As for inorganic photovoltaic cells, such as amorphous Si and GaAs cells, p^+n^+-tunneling ohmic junctions consisting of heavily doped pairs of semiconductors are generally used to connect *pn*- or *pin*-cells.[15-17] Recently, Timmreck et al. used a heavily doped organic *pn*-heterojunction as an ohmic interlayer.[18] In this study, the author chose C_{60} as a typical photovoltaic organic semiconductor and attempted to incorporate a tandem photovoltaic cell in single C_{60} films by doping only. For the ohmic interlayer, a heavily doped p^+n^+-C_{60} homojunction was used. For the unit cells, *pn*-C_{60} homojunction cells were used.[10] Molybdenum oxide (MoO_3)[9,10] and cesium carbonate (Cs_2CO_3)[19-21] were used as acceptor and donor dopants, respectively.

In this chapter, the author describes a tandem photovoltaic cell built into a single C_{60} film fabricated by doping only.

3.2. Experimental

C_{60} (Frontier Carbon, nanom purple TL) purified by single-crystal sublimation[6,22] was used. MoO_3 (Alfa Aeser, 99.9995%) and Cs_2CO_3 (Sigma-Aldrich, 99.995%) without further purification were used for the acceptor and donor dopants, respectively. **Fig. 3.1(a)** shows the structure of a tandem cell consisting of two *pn*-C_{60} unit cells (**Fig. 3.1(b)**). The C_{60} film was vacuum deposited on an indium tin oxide (ITO) substrate which was not exposed to oxygen plasma. Doping with MoO_3 and Cs_2CO_3 was performed by co-evaporation at 10^{-4} Pa in an oil-free vacuum evaporator (EpiTech Inc., ET300-6E-HK). Precise monitoring of the deposition rates of the dopants was achieved using quartz crystal microbalances equipped with a computer monitoring system (ULVAC, Depoview). To fabricate the *pn*-homojunctions, MoO_3 and Cs_2CO_3 dopants in volume concentrations of 3,000 (±200) and 500 (±20) ppm, respectively, were used. To make the n^+p^+-homojunction, both doping concentrations were increased to 50,000 ppm. Ohmic contacts to the ITO and Ag electrodes were formed by heavily doping 10 nm thick layers adjacent to the electrodes with MoO_3 (50,000 ppm) for the p^+ contact and Cs_2CO_3 (10,000 ppm) for the n^+ contact, respectively.[21] The Fermi levels (E_F) of the C_{60} film were measured using Kelvin vibrating capacitor apparatus (Riken-Keiki, FAC-1) without exposure to air at any time.

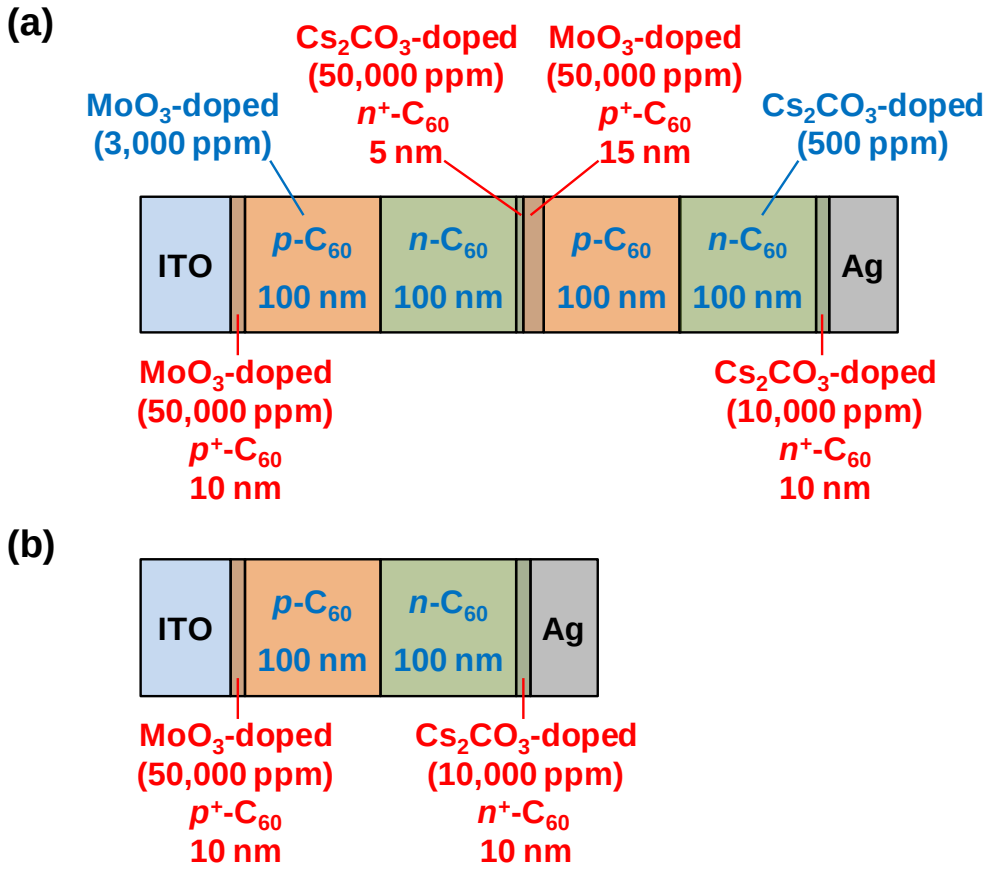

Fig. 3.1 (a) Structure of a tandem cell incorporating two *pn*-homojunction C_{60} cells connected by an n^+p^+-homojunction. (b) Structure of a unit cell incorporating a *pn*-homojunction.

3.3. Results and Discussion

3.3.1. Exploration of a Donor dopant

Since the aim of this thesis is the development of doping techniques for co-deposited films, the author searched for a donor dopant so that it can be applied to a co-deposited film consisting C_{60} and α-sexithiophene (6T). The donor dopant was explored among various materials, which can be deposited by vacuum evaporation. Lithium encapsulated fullerene (Li@C_{60}),[23,24] lithium fluoride (LiF),[25] ruthenium oxide (RuO_x), Calcium (Ca)[10] and Cs_2CO_3 (**Table 3.1**) were tested. For Li@C_{60}-doped, LiF-doped and RuO_x-doped C_{60} films, the E_Fs were not changed from the original E_F position of C_{60} (**Fig. 3.2(a)**). In contrast, for Ca-doped and Cs_2CO_3-doped C_{60} films, the E_Fs shifted negatively (**Fig. 3.2(b) and 3.2(c)**). These results mean that Ca and Cs_2CO_3 act as the donor dopants making C_{60} *n*-type. Actually, both Ca-doped and Cs_2CO_3-doped C_{60} films acted as *n*-type layers in *pn*-homojunctions formed in C_{60} films. However, for Ca-doped 6T film, 6T was decomposed to another material which gave out a sulfurous smell. On the other hand, for Cs_2CO_3-doped 6T films, there was no sign that 6T was decomposed. Thus, the author adopted Cs_2CO_3 as the donor dopant.

Table 3.1 Effect of doping with various materials.

Dopant	Shift in Fermi level of C_{60} by doping	Remarks
$Li@C_{60}$	No Shift	
LiF	No Shift	
RuO_x	No Shift	
Ca	Negative Shift	6T was decomposed by doping with Ca.
Cs_2CO_3	Negative Shift	Both C_{60} and 6T were not decomposed by doping with Cs_2CO_3.

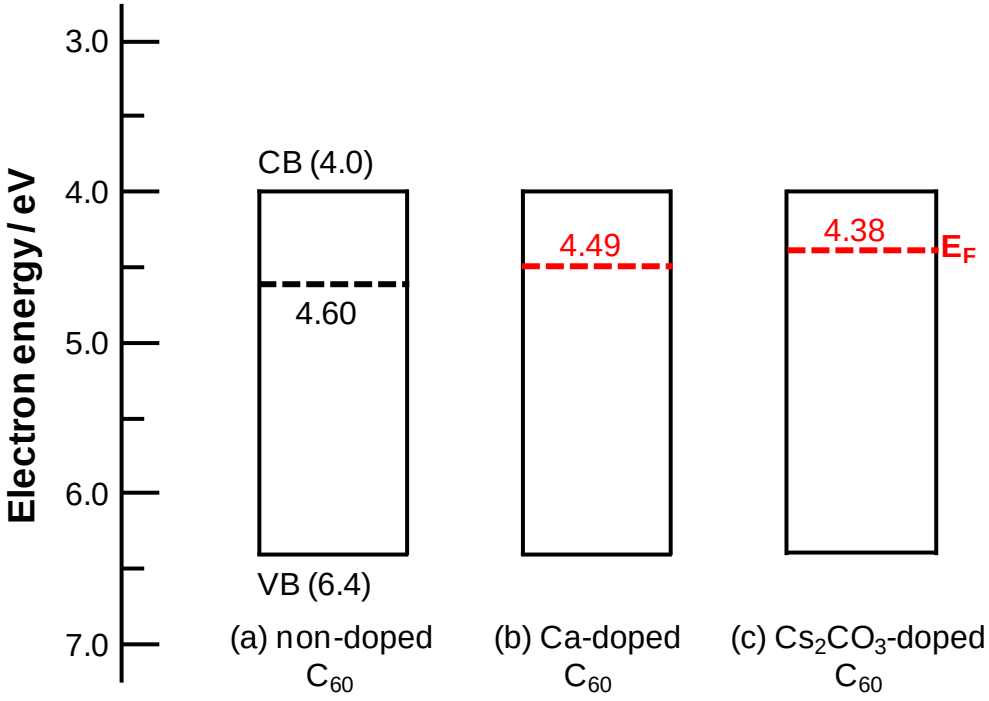

Fig. 3.2 Energy diagram of C_{60} for non-doped (a), Ca-doped (b) and Cs_2CO_3-doped films. The position of the upper edge of the valence band (VB) and the lower edge of the conduction band (CB) of C_{60} are determined by photoelectron spectroscopy and inverse photoelectron spectroscopy, respectively.

3.3.2. Control of Fermi Levels in Single C_{60} Films by Doping with MoO_3 and Cs_2CO_3

Fig. 3.3 shows the energy band diagrams of C_{60} films doped with MoO_3 and Cs_2CO_3. The values of the work functions of ITO, Ag, MoO_3, and Cs_2CO_3 films are also shown. For the 500 ppm Cs_2CO_3-doped C_{60} film, the E_F is located at 4.38 eV, which is close to the lower edge of the conduction band (CB) of C_{60} (4.0 eV).[26] A thick co-deposited film of C_{60}:Cs_2CO_3 in the ratio 10:1 changed the color to reddish brown and showed a new broad charge transfer (CT) absorption from the visible to the near infrared region. Since the work function of Cs_2CO_3 (2.96 eV) is more negative than the conduction band of C_{60} (4.0 eV), it is reasonable that Cs_2CO_3 donates an electron to C_{60} and forms a CT complex, i.e., C_{60}^----$Cs_2CO_3^+$. Here, the positive charge on the $Cs_2CO_3^+$ group can be regarded as a spatially fixed positive ion, i.e., an ionized donor. The negative charge on C_{60} can be liberated by thermal energy and acts as a free electron in the conduction band of C_{60}. Thus, the author concludes that Cs_2CO_3 acts as a donor dopant making C_{60} *n*-type. This donor property did not disappear even after exposure to air. When the doping concentration was increased to 50,000 ppm, E_F shifted slightly more negative (4.35 eV). On the other hand, for 3,000 and 50,000 ppm MoO_3-doped C_{60} films, the E_Fs are located at 5.88 and 5.97 eV, respectively, which are close to the upper edge of the valence band (VB) of C_{60} (6.4 eV). Formation of *p*-C_{60} by MoO_3 doping is caused by the opposite mechanism to Cs_2CO_3 doping.[9]

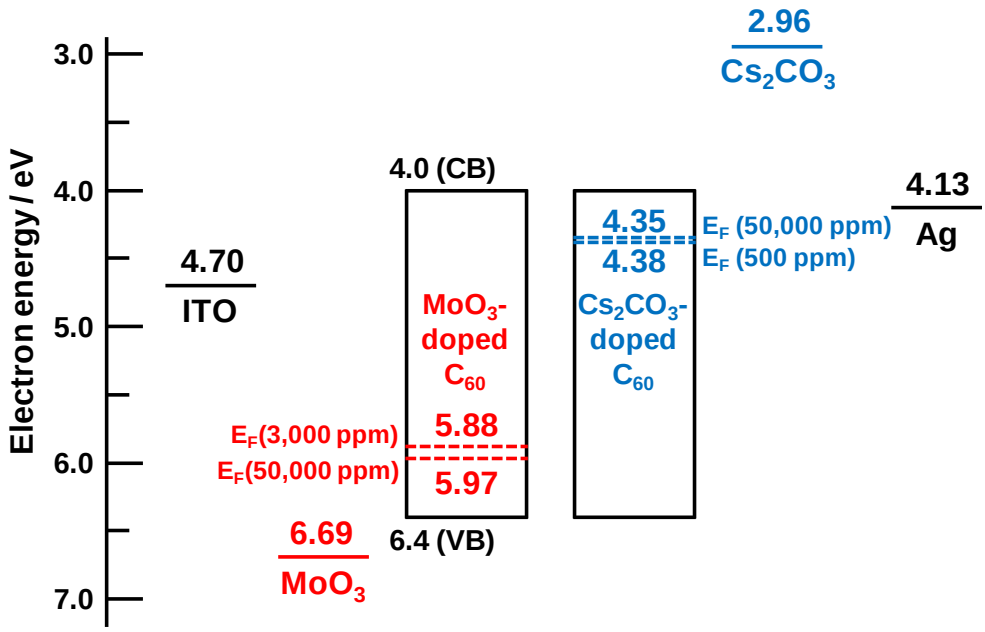

Fig. 3.3 Energy diagram of C_{60} films doped with MoO_3 and Cs_2CO_3. Values of the work functions of ITO, Ag, MoO_3, and Cs_2CO_3 are also shown.

3.3.3. n^+p^+-C_{60} Homojunction Acting as an Ohmic Interlayer

Curves A and B in **Fig. 3.4** show the current-voltage (*J*-*V*) characteristics for a tandem cell (**Fig. 3.4(a)**) and a unit cell (**Fig. 3.1(b)**), respectively. For the tandem cell, the V_{oc} value reaches 1.90 V. For the unit cell, the V_{oc} value is 1.03 V. V_{oc} has almost doubled (84% increase) by connecting two unit cells. When the n^+p^+-homojunction between the two unit cells of the tandem cell (**Fig. 3.1(a)**) was removed, V_{oc} remained the same (1.03 V), but the photocurrent density decreased significantly (curve C) compared to the unit cell (curve B). Thus, an n^+p^+-interconnecting homojunction is indispensable for doubling the V_{oc} value.

The short-circuit photocurrent density (J_{sc}) of the tandem cell was about a third of that of the unit cell since the magnitude of the photocurrent of the tandem cell was limited by the back cell operating under the light attenuated by the front cell. To overcome this, the values of J_{sc} generated by front and back cells should be equalized by equalizing the light absorption of the front and back cells having optimized thicknesses.

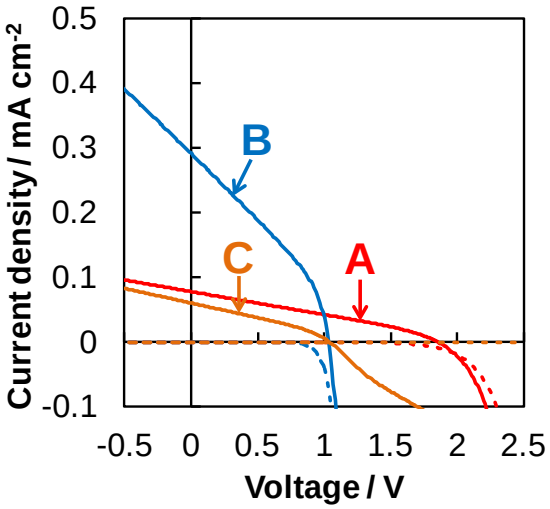

Fig. 3.4 Current-voltage (*J*-*V*) characteristics for the tandem cell (curves A)(Fig. 3.1(a)) and the unit cell (curves B)(Fig. 3.1(b)). Curves C are for a tandem cell without an n^+p^+-interconnecting homojunction. The photo and dark currents are shown by solid and broken curves, respectively. The ITO electrode was irradiated with simulated solar light (AM1.5, 100 mWcm^{-2}). Measurements were performed at 10^{-3} Pa. The short-circuit photocurrent, open-circuit photovoltage (V_{oc}), fill factor, and efficiency of the cells: (A) 0.09 mAcm^{-2}, 1.90 V, 0.29, 0.05%. (B) 0.29 mAcm^{-2}, 1.03 V, 0.34, 0.10%. (C) 0.06 mAcm^{-2}, 1.03 V, 0.32, 0.02%.

3.3.4. Energy Band Diagram of a Tandem C_{60} Photovoltaic Cell

In order to clarify the operating mechanism, energy band mapping of *pn*-homojunctions was performed using a Kelvin probe.[27,28] The positions of E_F for different film thicknesses near the *pn*-homojunction were measured from both sides of the junction interface. That is, the positions of E_F of Cs_2CO_3-doped C_{60} films deposited on MoO_3-doped C_{60} films (**Fig. 3.5(a)**) and also those of MoO_3-doped films deposited on Cs_2CO_3-doped films (**Fig. 3.5(b)**) were measured. The blue curves A in **Figs. 3.5(a)** and **3.5(b)** show the observed E_F values for MoO_3/Cs_2CO_3 doped homojunctions with concentrations of 3000/500 ppm, respectively. For the Cs_2CO_3 doped side (**Fig. 3.5(a)**), E_F gradually shifts more negatively, i.e., E_F gradually approaches the original E_F position of 500 ppm Cs_2CO_3-doped C_{60} (4.38 eV, see **Fig. 3.3**). This gradual shift extends beyond 100 nm. On the contrary, for the MoO_3-doped side (**Fig. 3.5(b)**), E_F gradually shifts more positively, i.e., E_F gradually approaches the original E_F position of 3,000 ppm MoO_3-doped C_{60} (5.88 eV, see **Fig. 3.3**). This gradual shift ends at around 30 nm. The profiles of the potential of the depletion layers formed on both sides of the homojunction can be depicted directly from the above complementary E_F observations.[29] Obviously, *pn*-homojunctions are drawn here (**Fig. 3.6**, blue shaded regions).

On the other hand, in the case of a heavily-doped homojunction, a narrower depletion layer is observed. The red curves B in **Figs. 3.5(a)** and **3.5(b)** show the observed E_F values for a MoO_3/Cs_2CO_3 homojunction doped with concentrations of 50,000/50,000 ppm. For the Cs_2CO_3 doped side (**Fig. 3.5(a)**), a rapid negative shift of E_F over the first 5 nm before reaching the original Fermi level position of 50,000 ppm Cs_2CO_3-doped C_{60} (4.35 eV, see **Fig. 3.3**) can be seen. For the MoO_3-doped side (**Fig.**

3.5(b)), there is a quick positive shift in E_F over 15 nm before it reaches the original Fermi level position of 50,000 ppm MoO_3-doped C_{60} (5.97 eV, see **Fig. 3.3**). Thus, an n^+p^+-homojunction (**Fig. 3.6**, red shaded region) connecting two *pn*-homojunctions (**Fig. 3.6**, blue shaded regions) is drawn.

The width of the depletion layers of the *pn*-homojunctions (blue shaded) and the n^+p^+-homojunction (red shaded) are 130 and 20 nm, respectively (**Fig. 3.6**). The former and the latter act as the active regions for photocurrent generation and the ohmic interlayer, respectively. Thus, the depletion layer width, which is closely related to the behavior of the homojunction, was controlled by the doping.

Suppression of the opposite photovoltage generated at the opposite *np*-homojunction between the two unit cells is strongly dependent on the thickness of the n^+p^+-homojunction. n^+/p^+ thicknesses of 5/15 nm (**Fig. 3.1(a)**) are the optimum values for which band bending ends within these regions (see **Fig. 3.5(a)** and **3.5(b)**, curves B). Actually, when the n^+p^+-thickness was decreased, V_{oc} decreased considerably due to the increase in the residual opposite *np*-homojunction.

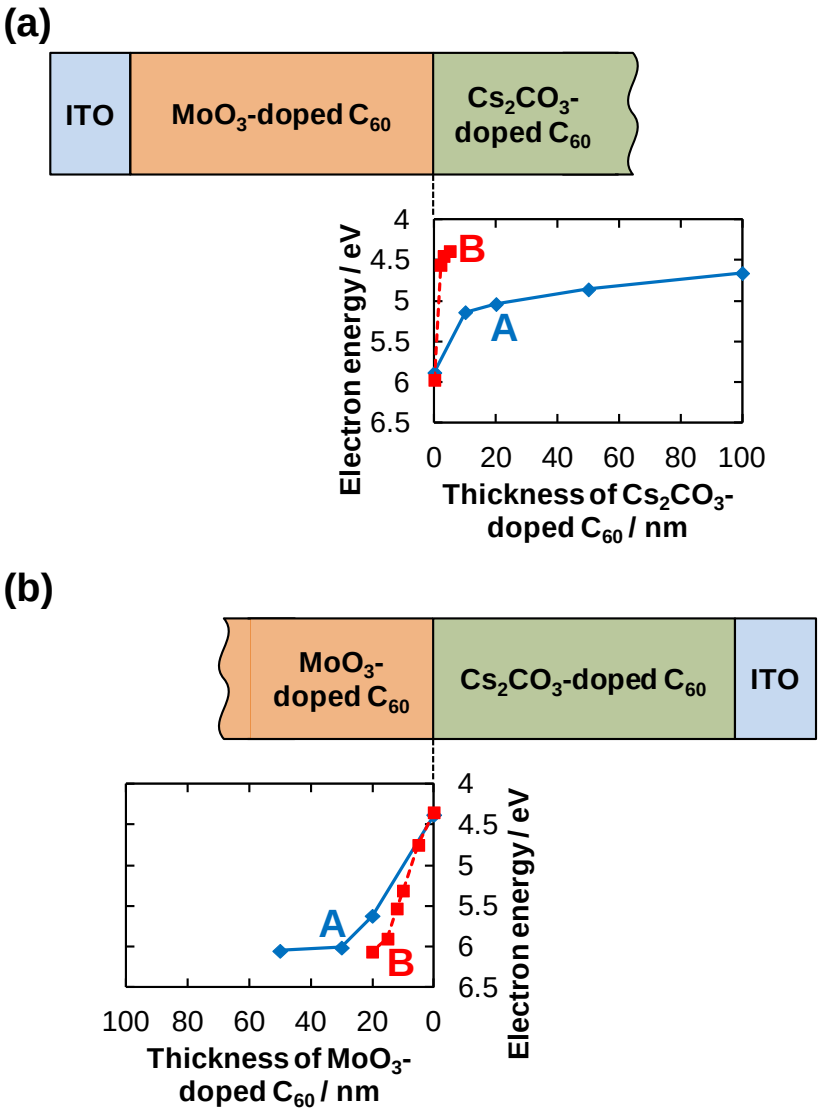

Fig. 3.5 Energy level mapping of *pn*-homojunctions using a Kelvin probe. Sample structures and the dependence of the position of the Fermi level on the thickness of a Cs_2CO_3-doped C_{60} film deposited on a MoO_3-doped C_{60} film (a) and a MoO_3-doped C_{60} film deposited on a Cs_2CO_3-doped C_{60} film (b) are shown. Curves A and B correspond to the different MoO_3/Cs_2CO_3 concentrations of 3000/500 ppm and 50000/50000 ppm, respectively.

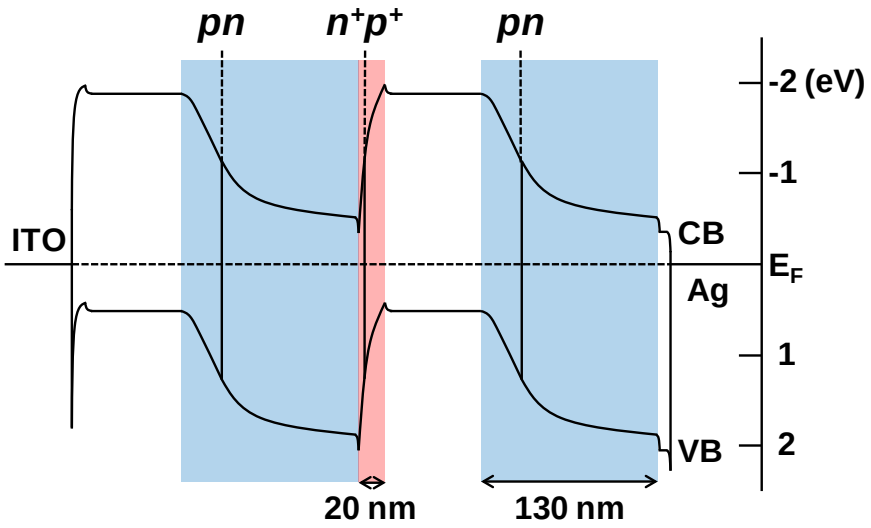

Fig. 3.6 Energy band diagram of a tandem cell based on Kelvin probe measurements (Fig. 3.5). The blue and red shaded regions correspond to the depletion layers for the *pn*- and n^+p^+-homojunctions, respectively.

3.4. Conclusion

In this chapter, a tandem photovoltaic cell was fabricated in a single film of C_{60} by connecting two *pn*-homojunctions with an n^+p^+-homojunction. The author thinks that the origin of the ohmic behavior of the n^+p^+-homojunction, which is a result of the disappearance of photogenerated electrons and holes, can be attributed to carrier recombination or tunneling. Optimization of the cell design is facilitated by reference to the energy band structure, which was precisely mapped using the Kelvin probe (**Fig. 3.6**).[30)]

3.5. References

1) Organic photovoltaics, Mechanisms, Materials and Devices, edited by S. –S. Sun and N. S. Sariciftci, published by CRC Press, New York, March (2005).

2) H. Spanggaard and F. C. Krebs, *Sol. Energy Mater. Sol. Cells*, **83**, 125 (2004).

3) H. Hoppe and N. S. Sariciftci, *J. Mater. Res*., **19**, 1924 (2004).

4) C. W. Tang, *Appl. Phys. Lett.*, **48**, 183 (1986).

5) M. Hiramoto, H. Fujiwara, and M. Yokoyama, *Appl. Phys. Lett.*, **58**, 1062 (1991).

6) M. Hiramoto and K. Sakai, *Mol. Cryst. Liq. Cryst*., **491**, 284 (2008).

7) T. Kaji, M. Zhang, S. Nakao, K. Iketaki, K. Yokoyama, C. W. Tang, and M. Hiramoto, *Adv. Mater.*, **23**, 3320 (2011).

8) W. E. Spear and P. E. Lecomber, *Solid State Commun.*, **17**, 1193 (1975).

9) M. Kubo, K. Iketaki, T. Kaji, and M. Hiramoto, *Appl. Phys. Lett.*, **98**, 073311 (2011).

10) M. Kubo, T. Kaji, and M. Hiramoto, *AIP Advances*, **1**, 032177 (2011).

11) M. Hiramoto, M. Suezaki, and M. Yokoyama, *Chem. Lett*., **19**, 327 (1990).

12) A. Yakimov and S. R. Forrest, *Appl. Phys. Lett*., **80**, 1667 (2002).

13) T. Ameri, G. Dennler, C. Lungenschmied, and C. J. Brabec, *Energy Environ. Sci*., **2**, 347 (2009) and the references therein.

14) G. Li, R. Zhu, and Y. Yang, *Nature Photon*., **6**, 153 (2012).

15) M. Ilegems, B. Schwartz, L. A. Koszi, and R. C. Miller, *Appl. Phys. Lett*., **33**, 629 (1978).

16) Y. Hamakawa, H. Okamoto, and Y. Nitta, *Appl. Phys. Lett*., **35**, 187 (1979).

17) C. Amano, H. Sugiura, A. Yamomoto, and M. Yamaguchi, *Appl. Phys. Lett*., **51**, 1998 (1987).

18) R. Timmreck, S. Olthof, K. Leo, and M. K. Riede, *J. Appl. Phys.*, **108**, 033108 (2010).

19) H.–H. Liao, L.–M. Chen, Z. Xu, G. Li, and Y. Yang, *Appl. Phys. Lett.*, **92** 173303 (2008).

20) S. Hamwi, T. Riedl, W. Kowalsky, *Appl. Phys. Lett.*, **99**, 053301 (2011).

21) M. Kubo, Y. Shinmura, N. Ishiyama, T. Kaji, and M. Hiramoto, *Appl. Phys. Express*, **5**, 092302 (2012).

22) R. A. Laudise, Ch. Kloc, P. G. Simpkins, and T. Siegrist, *J. Cyrstal Growth*, **187**, 449 (1998).

23) R. Tellgmann, N. Krawez, S.-H. Lin, I. V. Hertel, and E. E. B. Campbell, *Nature*, **382**, 407 (1996).

24) S. Aoyagi, E. Nishibori, H. Sawa, K. Sugimoto, M. Takata, Y. Miyata, R. Kitaura, H. Shinohara, H. Okada, T. Sakai, Y. Ono, K. Kawachi, K. Yokoo, S. Ono, K. Omote, Y. Kasama, S. Ishikawa, T. Komuro, and H. Tobita, *Nature Chem.* **2**, 678, (2010).

25) V. D. Mihailetchi, L. J. A. Koster, and P. W. M. Blom, *Appl. Phys. Lett.*, **85**, 970 (2004).

26) K. Walzer, B. Maennig, M. Pfeiffer, and K. Leo, *Chem. Rev.*, **107**, 1233 (2007).

27) N. Ishiyama, M. Kubo, T. Kaji, and M. Hiramoto, *Appl. Phys. Lett.*, **99**, 133301 (2011).

28) H. Ishii, K. Sugiyama, E. Ito, and K. Seki, *Adv. Mater.*, **11**. 605 (1999).

29) Only half the energy change of E_F in **Fig. 3.5** is plotted in the energy structure in **Fig. 3.6** because the depletion layer extends to both *p*- and *n*-type sides of the homojunction and the energy displacement is equally distributed to both sides.

30) For example, since there are dead layers in **Fig. 3.6** (not shaded regions), which attenuate the light, in front of the photoactive depletion layers in **Fig. 3.6** (blue shaded regions), J_{sc} values both for unit and tandem cells would increase by removing these dead layers, i.e., by decreasing the *p*-type C_{60} film thicknesses.

Chapter 4:

Control of the Conduction Types of Photovoltaic Co-deposited Films by Doping with Molybdenum Oxide

"Doping-based control of the energetic structure of co-deposited films", Norihiro Ishiyama, Masayuki Kubo, Toshihiko Kaji, and Masahiro Hiramoto, *Applied Physics Letters*, **99**, 133301 (2011).

Abstract

Control of the energy structure of photovoltaic co-deposited films consisting of fullerene and α-sexithiophene was demonstrated by ppm-level doping with molybdenum oxide (MoO_3). The transition from an *n*-type Schottky junction *via* a metal/insulator/metal junction to a *p*-type Schottky junction by increasing the MoO_3 doping concentration was verified by observing the photovoltaic properties. Direct ppm-level doping into photoactive co-deposited films could become a powerful tool for designing the appropriate built-in potential for efficient organic photovoltaic cells.

4.1. Introduction

Recent small-molecular-type organic solar cells[1-4] incorporate co-deposited films consisting of two kinds of organic semiconductors, which is an indispensable technique for generating significant photocurrent densities based on the dissociation of excitons by the photoinduced electron transfer process.[5-7]

On the other hand, *pn*-control in highly-purified semiconductors by adding a small amount of dopants is potentially important for organic solar cells.[8-10] As for inorganic solar cells, energy structures like *pn*-homojunctions, which create a 'built-in' potential, have been intentionally designed based on a technique involving *pn*-control by doping.[11] Recently, Kubo et al. reported *pn*-control by doping and *pn*-homojunction formation for single fullerene (C_{60}) films.[12,13]

For the photoactive co-deposited films themselves, however, there has so far been no attempt to achieve *pn*-control by doping. The author believes that the formation of a *pn*-homojunction directly in the bulk of co-deposited films has high potential to enhance the efficiency of cells. In this study, the author adopted a co-deposited film consisting of α-sexithiophene (6T) and C_{60} since this combination exhibits a large open-circuit voltage, reaching 0.9 V.[14] As a dopant, molybdenum oxide (MoO_3), which acts as an acceptor,[12,13,15] was used.

In this chapter, the author describes a technique that enables control of the internal energy structure of co-deposited films by MoO_3-doping.

4.2. Experimental

C_{60} (Frontier Carbon, nanom purple TL) and 6T (Tokyo Chemical Industry) samples were purified by single-crystal formed sublimation under flowing N_2 at 1 and 0.1 atm, respectively.[16] The purity of the C_{60} crystals was determined by secondary ion mass spectroscopy to seven-nines (7N; 99.99999%; impurity concentration < 0.1 ppm).[17,18] MoO_3 (Alfa Aeser, 99.9995%) was used as a dopant.

The structure of the cells is shown in **Fig. 4.1**. Co-deposited (C_{60}:6T) films of 650 nm in thickness were deposited on indium tin oxide (ITO) glass substrate under 10^{-4} Pa pressure using an oil–free vacuum evaporator (ULVAC, VTS-350M/ERH). The ratio of C_{60} to 6T was maintained at 0.97 to 0.03. MoO_3 (10 nm)/Ag (100 nm) was deposited as a counter electrode.

Doping of MoO_3 into the C_{60}:6T co-deposited films was performed by using the 'three component co-evaporation' technique (**Fig. 4.2**). The thicknesses of the C_{60}, 6T, and MoO_3 were monitored independently by using three quartz crystal monitors (QCM; ULVAC, CRTM-6000G). Precise monitoring of the deposition rate of the MoO_3 at 1.4 x 10^{-5} nms^{-1} was achieved by using a QCM equipped with a computer monitoring system (ULVAC, Depoview) which allowed us to dope with MoO_3 to as low as 70 ppm in volume concentration (**Fig. 4.3**). In the present study, the MoO_3-doping concentrations were 0 (non-doped), 400, 600, 1100, 4300 ppm.

The Fermi levels (E_F) of the organic films were measured without exposing the films to air by using a Kelvin probe (Riken-Keiki, FAC-1) in a glove box.[12] Action spectra were measured by irradiating monochromatic light from a Xe-lamp through a monochromator under a vacuum of 10^{-4} Pa.

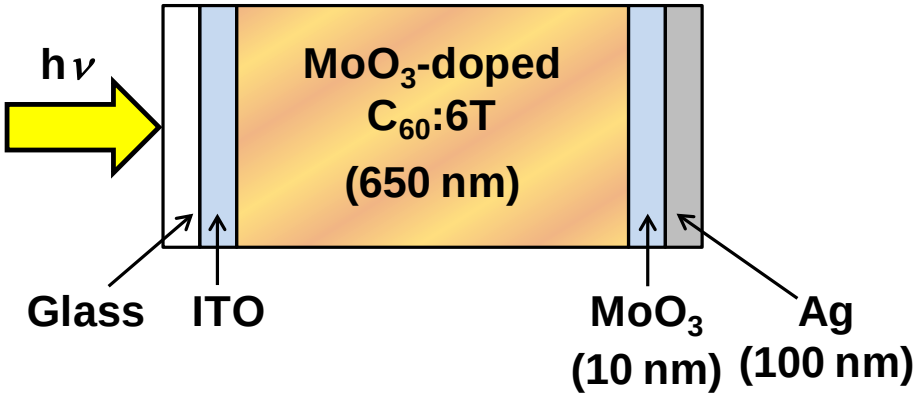

Fig. 4.1 Cell structure of an MoO_3-doped C_{60}:6T co-deposited film (650 nm) sandwiched between ITO and MoO_3/Ag electrodes. The doping concentrations of MoO_3 by volume are 0 (non-doped), 400, 600, 1100, and 4300 ppm.

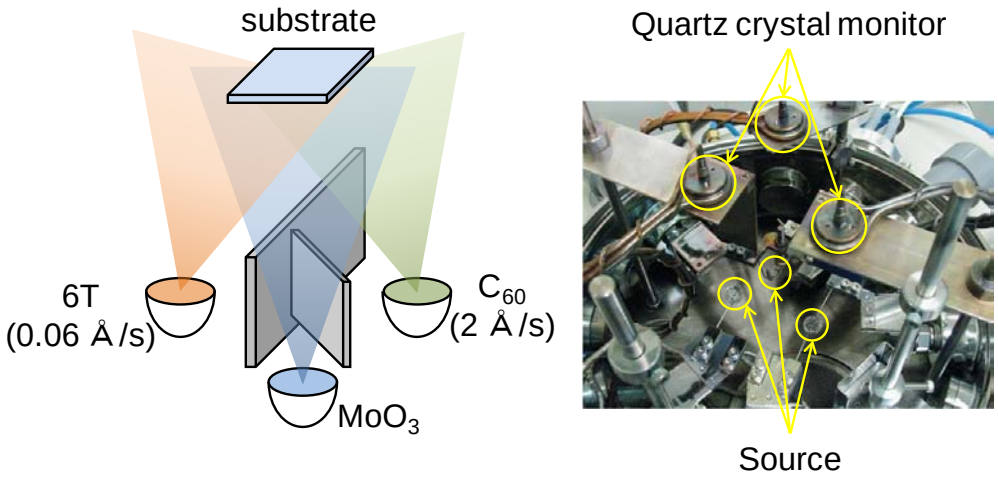

Fig. 4.2 Equipment for a 'three component co-evaporation' technique.

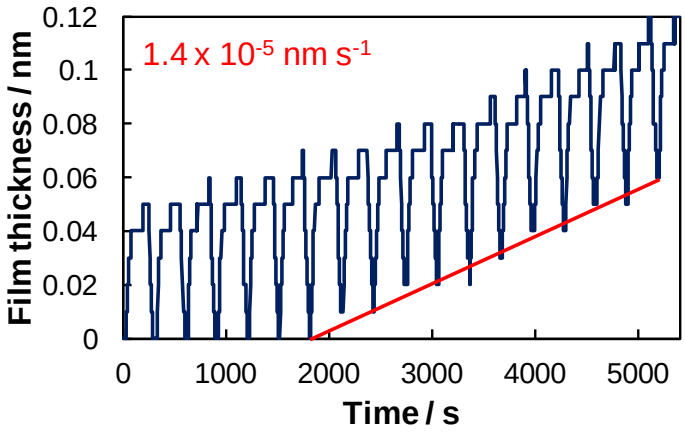

Fig. 4.3 Precise monitoring of deposition rate using a computer monitoring system. The distances from the MoO_3 source to the QCM and to the substrate were 9 and 18 cm, respectively. The tooling factor as determined by the surface profilometer was 0.25. The relationship between the total-thickness signal from the QCM vs. time was monitored using a PC display. For 70 ppm Cs_2CO_3, there was a very slow cyclic fluctuation (frequency: ~300 s, amplitude: ~0.05 nm) caused by temperature variations in the coolant water for the QCM. A reproducible increase in the baseline of 0.06 nm, which was only noted during MoO_3 evaporation over a prolonged timescale of 4300 seconds, was observed (1.4×10^{-5} nm s^{-1}).

4.3. Results and Discussion

4.3.1. Positive Shift of Fermi Level in a Co-deposited Film Consisting of C_{60} and α-Sexithiophene (C_{60}:6T) by MoO_3 Doping

Fig. 4.4 shows the energy diagrams of C_{60}[19] and 6T single films and of a C_{60}:6T co-deposited film together with the work functions of MoO_3 and ITO.[20] The measured value of E_Fs for MoO_3 doping concentrations of 0 ppm (non-doped)(blue broken line) and 3000 ppm (red broken line) are shown. For both C_{60} and 6T single films, E_F shifted positively and reached close to the valence band (VB) when the MoO_3-doping was 3000 ppm. On the other hand, both co-deposited films of C_{60}:MoO_3 and 6T:MoO_3 of 1:1 ratio showed a strong new charge-transfer (CT) absorption from the visible to the near-infrared due to the work function of MoO_3 (6.69 eV), which is considerably more positive than the energy locations of VB for C_{60} (6.4 eV) and 6T (5.3 eV). This result means that the CT complexes C_{60}^{+}---MoO_3^{-} and $6T^{+}$---MoO_3^{-} are formed in the MoO_3-doped films. Here, negative charges are the 'spatially-fixed' ionized MoO_3 acceptors. The positive charges on C_{60}^{+} and $6T^{+}$ can be liberated from the negative charges by heat at room temperature, and can then move as free holes in VB. Based on these results, the author concluded that the conduction type of 6T and C_{60} films is changed to *p*-type.

It should be noted that the present MoO_3 dopant has the ability to act as an acceptor for both of the organic semiconductors that compose a C_{60}:6T co-deposited film. Actually, a positive shift of E_F was observed for a C_{60}:6T co-deposited film (**Fig. 4.4**). This suggests that, by MoO_3-doping, the conduction type of the co-deposited film changed from *n*- to *p*-type as a whole.[21]

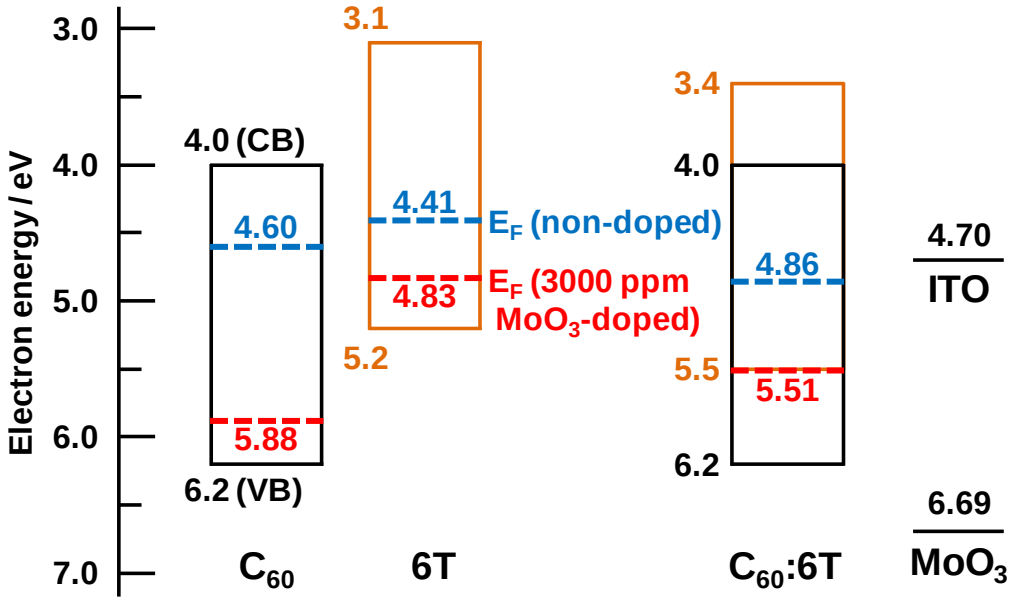

Fig. 4.4 Energy diagrams of C_{60} and 6T single films and a C_{60}:6T co-deposited film. C_{60} and 6T are shown by the black and orange lines, respectively. CB and VB denote the conduction band and the valence band, respectively. The work functions of MoO_3 and ITO are also shown. The values of E_Fs for a non-doped (0 ppm) film and for a 3000 ppm MoO_3-doped film are indicated by the blue and red broken lines, respectively.

4.3.2. Tuning of Conduction Type in C_{60}:6T Films by MoO_3 Doping

Fig. 4.5 shows the action spectra of the external quantum efficiency (EQE) of the short-circuit photocurrent under light irradiation to the ITO electrode. The black curve shows the absorption spectrum of the cells. In the cases of non-doped (0 ppm) and 400 ppm MoO_3-doped cells (**Fig. 4.5**, curves A and B), photocurrent appeared in the region from 500 to 700 nm, where there is weak absorption from the cells. Since light was irradiated onto the side with the ITO electrode, this means that the light was transmitted into the cell bulk and reached close to the opposite MoO_3/Ag electrode, generating the photocurrent (masking effect). Taking the observed result that direction of the photovoltage in all of the present cells was such that the ITO was minus and the MoO_3/Ag was plus into account, then an *n*-type Schottky junction was formed at the C_{60}:6T/MoO_3 interface (**Fig. 4.6(a)**). Namely, C_{60}:6T co-deposited films behave as *n*-type.

In the case of the 600 ppm-doped cell (**Fig. 4.5**, curve C), the photocurrent was distributed equally throughout the wavelength region from 300 to 700 nm, irrespective of the magnitude of the absorbance. Since light was absorbed by both the ITO side for the strong absorption region (300-500 nm) and at the MoO_3/Ag side for the weak absorption region (500-700 nm), this observation indicates that the generation of photocurrent occurs in the whole of the bulk of the cell. Namely, the co-deposited film behaves as 'intrinsic' material (**Fig. 4.6(b)**). In other words, the inherent *n*-type nature of the non-doped C_{60}:6T film is compensated by a low concentration (600 ppm) of doping with MoO_3.

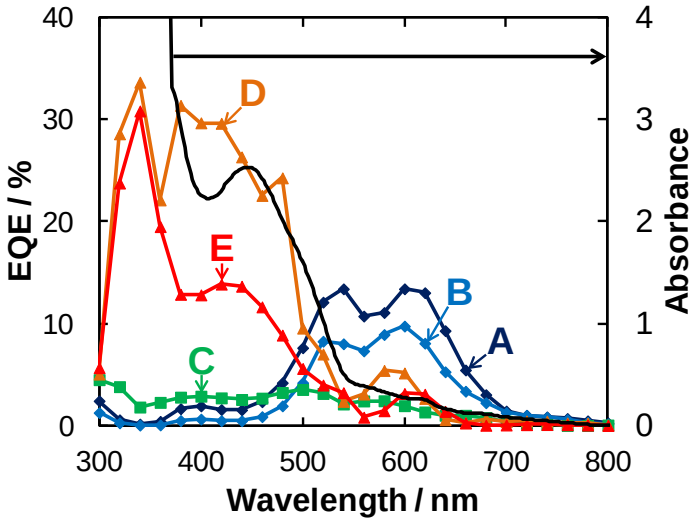

Fig. 4.5 Action spectra of the external quantum efficiency (EQE) of the short-circuit photocurrent for the cells in Fig. 4.1 under irradiation onto the ITO electrodes. Curves A to E correspond to MoO_3-doping concentrations of 0 (non-doped), 400, 600, 1100, and 4300 ppm, respectively. The absorption spectrum of the cell is shown by the black curve.

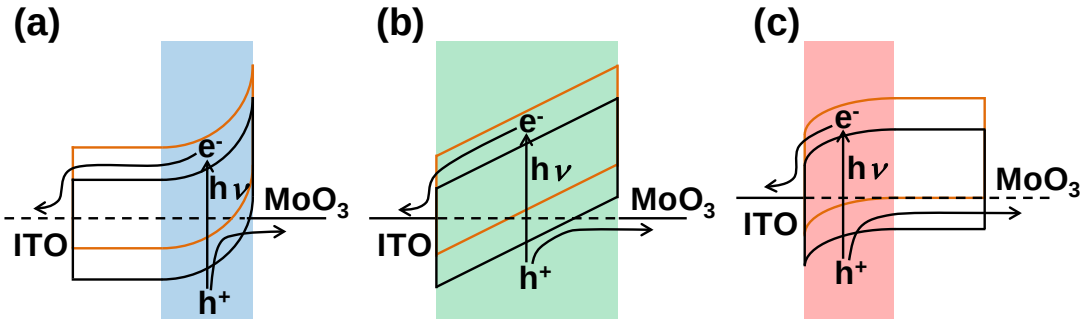

Fig. 4.6 Schematic energy band diagrams of the ITO/C_{60}:6T/MoO_3 cells for various MoO_3-doping concentrations. (a) 0 (non-doped) and 400 ppm. (b) 600 ppm. (c) 1100 and 4300 ppm. C_{60} and 6T are shown by the black and orange lines, respectively. The shaded areas correspond to the active zones for photocurrent generation. Photocurrent generation by the C_{60} excitation is also shown.

In the case of 1100 and 4300 ppm-doped cells (**Fig. 4.5**, curves D and E), action spectra appeared in the strong absorption region (300–500 nm), where absorption occurred near to the ITO electrode. Taking the same direction of photovoltage (-:ITO, +:Ag) into account as before, this means that a *p*-type Schottky junction was formed at the ITO/C_{60}:6T interface (**Fig. 4.6(c)**). Namely, the C_{60}:6T films behave as *p*-type.[22)]

Fig. 4.7 shows the dependence of the magnitude of the forward dark-current density at +1 V on the MoO_3-doping concentration. It initially decreased with MoO_3-doping and reached a minimum at 600 ppm, but then it increased steeply again with rising doping concentration. Obviously, compensation of the inherent electron conduction in a C_{60}:6T film due to hole-conduction caused by a low-level of doping with MoO_3 (600 ppm) occurs. For higher doping concentrations, hole-concentration dominates the conduction regime. This observation coincided well with the observed transition of conduction type, i.e., *n*-type (**Fig. 4.6(a)**), intrinsic (**Fig. 4.6(b)**), and *p*-type (**Fig. 4.6(c)**).

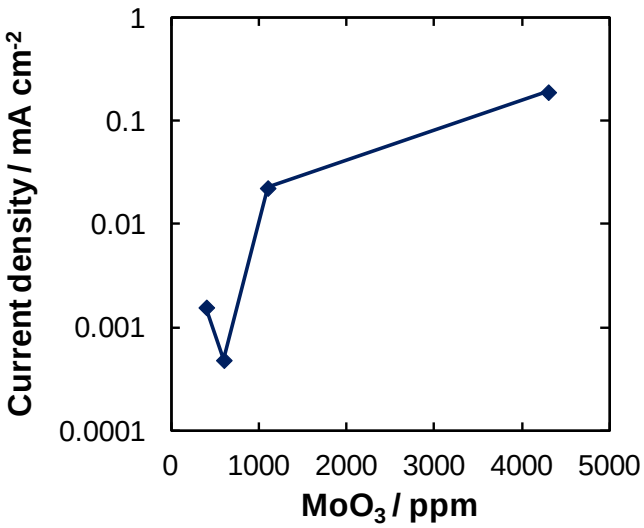

Fig. 4.7 Dependence of the magnitude of forward dark current density at +1 V on MoO_3-doping concentration.

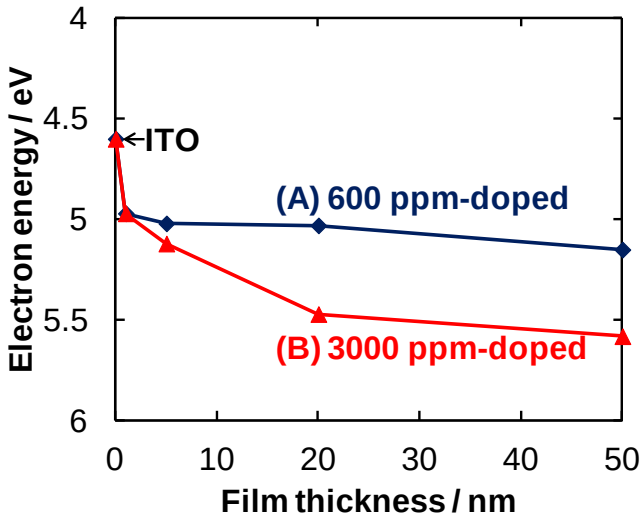

Fig. 4.8 Dependence of E_F position on film thicknesses near the ITO contacts for 600 (curve A) and 3000 ppm (curve B) MoO_3-doped C_{60}:6T films.

4.3.3. Potential Profiles of MoO_3-doped C_{60}:6T Cells

The author measured the E_F position for different film thicknesses near the ITO contacts by using the Kelvin probe for 600 and 3000 ppm MoO_3-doped samples (**Fig. 4.8**). Abrupt drop within 5 nm can be attributed to the interfacial dipole layer formation.[23] Above 5 nm, for 600 ppm doped film, E_F maintained constant, i.e., C_{60}:6T acts as insulator. Thus, potential profile in **Fig. 4.6(b)** can be drawn. For 3000 ppm doped film, E_F gradually shifted positively, i.e., E_F approached gradually to the VB of 6T:C_{60}. Thus, potential profile in **Fig. 4.6(c)**, which is upside-down to **Fig. 4.8** (curve B), can be drawn.

The energy band diagrams after contacting for the ITO/C_{60}:6T/MoO_3 cells shown in **Fig. 4.6** can be depicted based on the energy relationships between E_Fs for C_{60}:6T and the work functions of ITO and MoO_3 shown in **Fig. 4.4**. For a non-doped C_{60}:6T cell (E_F; blue broken line), ohmic and *n*-type Schottky junctions are formed at the ITO/C_{60}:6T and the C_{60}:6T/MoO_3 contacts, respectively. For the 3000 ppm MoO_3-doped C_{60}:6T cell, *p*-type Schottky and ohmic junctions are formed at the ITO/C_{60}:6T and the C_{60}:6T/MoO_3 contacts, respectively.

4.4. Conclusion

In this chapter, the internal energy structures of C_{60}:6T co-deposited films were intentionally tuned from *n*-type Schottky junctions through metal/intrinsic/metal junctions to *p*-type Schottky junctions by doping with MoO_3.

4.5. References

1) Organic photovoltaics, Mechanisms, Materials and Devices, edited by S.–S. Sun and N. S. Sariciftci, published by CRC Press, New York, March (2005).

2) H. Spanggaard and F. C. Krebs, *Sol. Energy Mater. Sol. Cells*, **83**, 125 (2004).

3) H. Hoppe and N. S. Sariciftci, *J. Mater. Res*., **19**, 1924 (2004).

4) C. W. Tang, *Appl. Phys. Lett.*, **48**, 183 (1986).

5) M. Hiramoto, H. Fujiwara, and M. Yokoyama, *Appl. Phys. Lett.*, **58**, 1062 (1991).

6) M. Hiramoto, H. Fujiwara, and M. Yokoyama, *J. Appl. Phys.*, **72**, 3781 (1992).

7) K. Suemori, T. Miyata, M. Yokoyama, and M. Hiramoto, *Appl. Phys. Lett.*, **86**, 063509 (2005).

8) M. Hiramoto, Y. Kishigami, and M. Yokoyama, *Chem. Lett.*, **19**, 119 (1990).

9) M. Hiramoto, K. Ihara, H. Fukusumi, and M. Yokoyama, *J. Appl. Phys.*, **78**, 7153 (1995).

10) K. Walzer, B. Maennig, M. Pfeiffer, and K. Leo, *Chem. Rev.*, **107**, 1233 (2007).

11) W. E. Spear and P. E. Lecomber, *Solid State Commun.*, **17**, 1193 (1975).

12) M. Kubo, T. Kaji, K. Iketaki, and M. Hiramoto, *Appl. Phys. Lett.*, **98**, 073311 (2011).

13) M. Kubo, T. Kaji, and M. Hiramoto, AIP Advances, 1, 032177 (2011).

14) J. Sakai, T. Taima, and K. Saito, *Organic Electronics*, **9**, 582 (2008).

15) T. Matsushima, Y. Kinoshita, and H. Murata, *Appl. Phys. Lett.*, **91**, 253504 (2007).

16) R. A. Laudise, Ch. Kloc, P. G. Simpkins, and T. Siegrist, *J. Crystal Growth*, **187**, 449 (1998).

17) M. Hiramoto and K. Sakai, *Mol. Cryst. Liq. Cryst.*, **491**, 284 (2008).

18) M. Hiramoto, Proceedings of SPIE, Vol. 7052, Organic Photovoltaics IX,

pp70520H-1-6, San Diego, CA, USA, 12-14 August (2008).

19) C. Falkenberg, C. Uhrich, S. Olthof, B. Maennig, M. Riede, and K. Leo, *J. Appl. Phys*., **104**, 034506 (2008).

20) VB position of 6T in C_{60}:6T co-deposited film (5.5 eV) was different to single 6T film (5.2 eV) presumably due to the existence of 6T single molecules or tiny 6T aggregates, which interacts with C_{60}.

21) When one assumes the phase separation of 6T and C_{60}, the energy structure of the bulk of a co-deposited layer such as 6T/C_{60}/6T/C_{60} can be depicted based on the measured values of E_Fs for C_{60} and 6T single layers and for a C_{60}:6T co-deposited layer. For the MoO_3-doped *p*-type case, holes are suggested to be mainly transported through the 6T region.

22) By increasing the doping concentration from 1100 to 4300 ppm, the shortest wavelength peak where absorbance exceeds 3 (300 - 400 nm) became the main component. Obviously, the depletion layer of the *p*-type Schottky junction, shrunk with increasing doping concentration.

23) H. Ishii, K. Sugiyama, E. Ito, and K. Seki, *Adv. Mater*., **11**, 605 (1999).

Chapter 5:

Control of the Barrier Parameters of *n*-Type Schottky Junctions in Photovoltaic Co-deposited Films by Doping with Cesium Carbonate

"Tuning of Barrier Parameters of n-Type Schottky Junctions in Photovoltaic Co-Deposited Films by Doping", Norihiro Ishiyama, Tadashi Yoshioka, Toshihiko Kaji, and Masahiro Hiramoto, *Appl*. *Phys*. *Express*, **6**, 012301 (2013).

Abstract

Tuning of the barrier parameters of *n*-type Schottky junctions formed in photovoltaic co-deposited films consisting of fullerene and α-sexithiophene (C_{60}:6T) was demonstrated by ppm-level control of cesium carbonate (Cs_2CO_3) doping. Increases in the carrier concentration of electrons along with the overall doping concentration, which was observed by capacitance measurements and which affected cell performance, confirmed that Cs_2CO_3 acts as donor dopant for C_{60}:6T co-deposited films. The doping efficiency was determined to be around 0.15.

5.1. Introduction

Controlling the energy structure by impurity doping is a matter of great importance for small-molecular-type organic photovoltaic cells[1-8], just as it is in the case of inorganic cells.[9] Complete *pn*-control and *pn*-homojunction formation in both single fullerene (C_{60})[10,11] and metal-free phthalocyanine films[12] have been reported. On the other hand, co-deposited films consisting of two kinds of organic semiconductors are essential components to generate significant photocurrent densities, based on the photoinduced exciton dissociation process.[5-8] In **chapter 4**, the author developed a direct doping technique for co-deposited films consisting of C_{60} and α-sexithiophene (C_{60}:6T)[13] and fabricated *p*-type C_{60}:6T co-deposited films by doping with molybdenum oxide (MoO_3), which acts as an acceptor.[14] In this study, the author chose cesium carbonate (Cs_2CO_3) as the donor dopant[15-17] and attempted to control the barrier shape of Schottky junctions formed in C_{60}:6T co-deposited films. To determine the barrier parameters, low-frequency capacitance measurements[18,19] were employed.

In this chapter, the author describes the intentional tuning of the barrier parameters of *n*-type C_{60}:6T Schottky junctions by changing the doping concentration of Cs_2CO_3.

5.2. Experimental

C_{60} (Frontier Carbon, nanom purple TL) and 6T (Tokyo Chemical Industry) samples purified by single-crystal sublimation[6,20] under flowing N_2 at 1 and 0.1 atm, respectively, were used to fabricate the junctions. Cs_2CO_3 (Sigma-Aldrich, 99.995%) was used without further purification as the donor dopant. **Fig. 5.1(a)** shows the structure of Schottky cells formed using C_{60}:6T co-deposited films. The C_{60}:6T films were deposited on indium tin oxide (ITO) glass substrates at 10^{-4} Pa in an oil-free vacuum evaporator (EpiTech Inc., ET300-6E-HK). The ratio of C_{60} to 6T was maintained at 10 to 1.[13,14] Doping of Cs_2CO_3 into the C_{60}:6T was performed using a 'three component co-evaporation' technique.[14] Precise monitoring of the deposition rate of Cs_2CO_3 at 1 x 10^{-5} nm s^{-1} was achieved using quartz crystal microbalances equipped with a computer monitoring system (ULVAC, Depoview), which allowed us to dope Cs_2CO_3 as low as 40 ppm by volume concentration. Doping at concentrations of 40, 150, and 500 ppm was performed. Low-frequency capacitance measurements[18,19] were performed under vacuum (10^{-3} Pa). A periodical triangular bias was applied to the cells by using a function generator (Hokuto Denko, HB-102) and the dark current was measured using a picoammeter (Keithley 485). Fermi level (E_F) measurements were performed by using a Kelvin vibrating capacitor apparatus (Riken-Keiki, FAC-1) without exposure to air at any time.

5.3. Results and Discussion

5.3.1. Formation of Cs_2CO_3-doped n-Type C_{60}:6T Schottky Junctions

Fig. 5.1(b) shows the spectral dependence of the external quantum efficiency (EQE). Under irradiation onto the ITO electrode, a photocurrent (curves A, B, and C) appeared in the strong absorption region of the cell (black curve). This means that the photoactive region is located towards the light-irradiated side, i.e., at the MoO_3/C_{60}:6T interface.[21] Taking into consideration that the photovoltage of ITO/MoO_3 is positive and that of bathocuproine (BCP)/Ag is negative, Schottky barriers were obviously formed at the interfaces between the MoO_3 and the C_{60}:6T films, showing *n*-type nature due to Cs_2CO_3 doping.[22]

Fig. 5.1(c) shows the current-voltage characteristics for cells with Cs_2CO_3 doping concentrations of 40 (curve A), 150 (curve B), and 500 (curve C) ppm. The magnitude of the forward current density increased with increasing doping concentration (broken curves). In addition, the fill factor increased slightly as the doping concentration increased from 40 to 150 ppm (solid curves A and B, respectively). These results suggest that the bulk resistances of the C_{60}:6T cells were reduced by Cs_2CO_3 doping. On the other hand, further increase in the doping concentration from 150 to 500 ppm (solid curves B and C) caused a reduction in the photocurrent by about half. Simultaneously, the EQE values also decreased (**Fig. 5.1(b)**, curves A, B, and C). These results suggest that the widths of the photoactive Schottky barriers shrunk with increasing doping concentration.

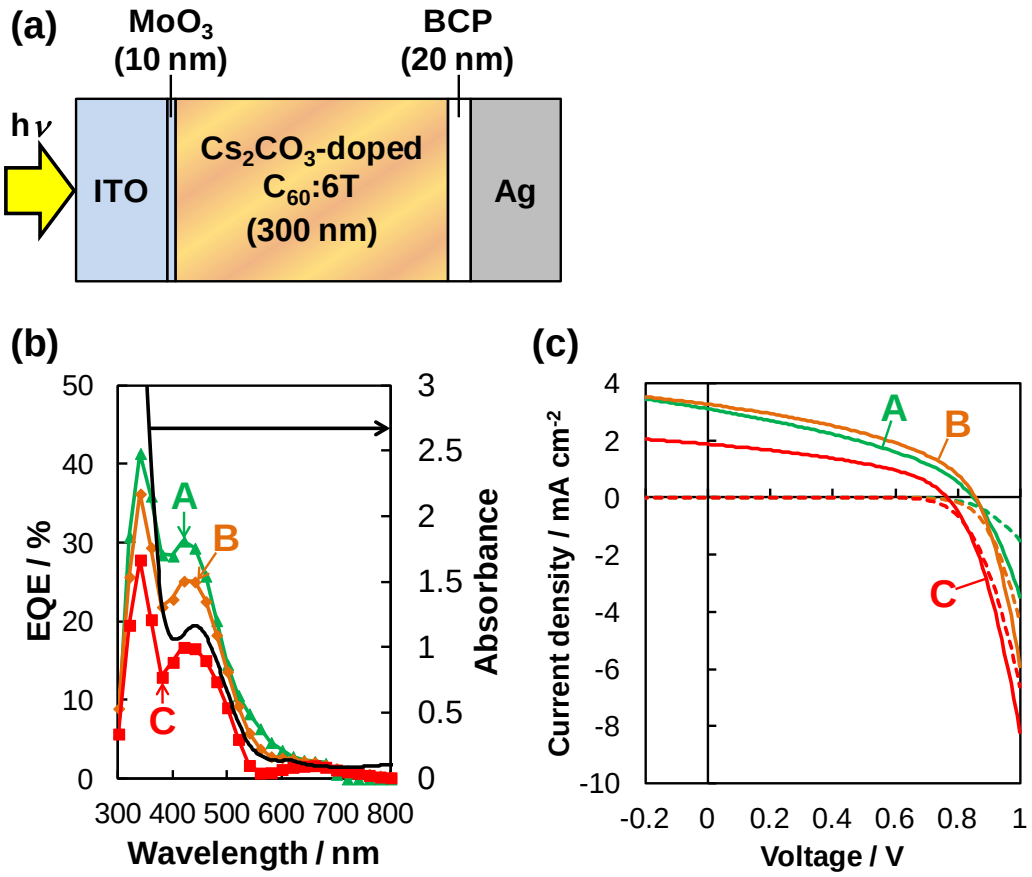

Fig. 5.1 (a) Structure of Cs_2CO_3-doped C_{60}:6T cells. (b) Action spectra of the external quantum efficiency (EQE) for the short-circuit photocurrent. The black curve shows the absorption spectrum of the cell. (c) Current-voltage characteristics. The photo and dark currents are shown by the solid and broken curves, respectively. Simulated solar light (AM 1.5, 100 mW cm^{-2}) was irradiated onto the ITO electrode. Curves A, B, and C correspond to Cs_2CO_3 doping concentrations of 40, 150, and 500 ppm, respectively. The measurements were performed at 10^{-3} Pa.

5.3.2. Barrier Parameters and Doping Efficiency in Cs_2CO_3-doped C_{60}:6T Cells

So, as a next step, the author performed low-frequency capacitance measurements[18,19] to determine the barrier parameters of the Schottky junctions formed at the MoO_3/*n*-C_{60}:6T interfaces. **Fig. 5.2(a)** shows a typical dark current-voltage curve measured at a scanning rate of 5 V s^{-1}. Clear hysteresis was observed. Since the magnitude of the displacement current was dependent on the Cs_2CO_3 doping concentration, the observed hysteresis can be attributed to charging to and discharging from the depletion layer of the Schottky junction formed at the MoO_3/C_{60}:6T interface by Cs_2CO_3 doping.

From **Fig. 5.2(a)**, the differential capacitance ($C_d(V)$) can be obtained using **Eq. (5.1)**.

$$C_d = \Delta I(V)/8V_0 f \qquad (5.1)$$

Here, $\Delta I(V)$, $2V_0$, and f are the current difference due to the hysteresis, the range of the applied bias, and the frequency of the periodical triangular bias, respectively (see **Fig. 5.2(a)**). **Fig. 5.2(b)** shows the Mott-Schottky plots (C_d^{-2}-V) for doping concentrations of 40 (curve A), 150 (curve B), and 500 (curve C) ppm. Clear linear relationships were obtained for all cells. From the slope of the curves, carrier concentrations for electrons (N_D) were calculated based on **Eq. (5.2)** by assuming a relative dielectric constant (ε) of 4.4 for C_{60}.[23]

$$C_d^{-2}(V) = 2(V - V_{bi})/eN\varepsilon\varepsilon_0 \qquad (5.2)$$

From the C_d values at zero bias (V=0), the depletion layer width (W_{dep}) was calculated based on **Eq. (5.3)**.

$$C_d(V = 0) = \varepsilon\varepsilon_0/W_{dep} \qquad (5.3)$$

The built-in potential (V_{bi}) was obtained from the intercept of the x-axis.

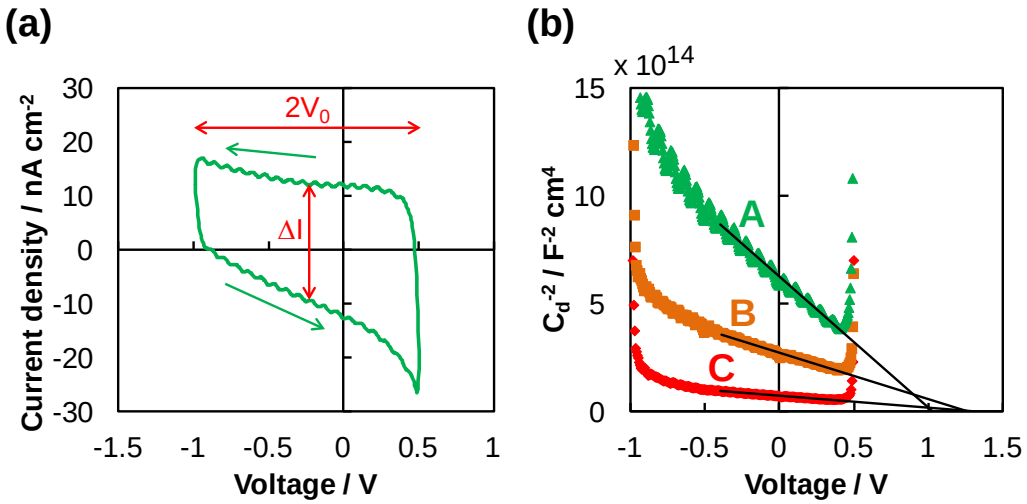

Fig. 5.2 (a) Dark current-voltage curve obtained by applying a triangular bias at a scanning speed of 5 V s^{-1} for a 40 ppm Cs_2CO_3-doped cell. (b) Mott-Schottky plots for the doping concentrations of 40 (curve A), 150 (curve B), and 500 (curve C) ppm. The measurements were performed using exactly the same cells as those in Fig. 5.1.

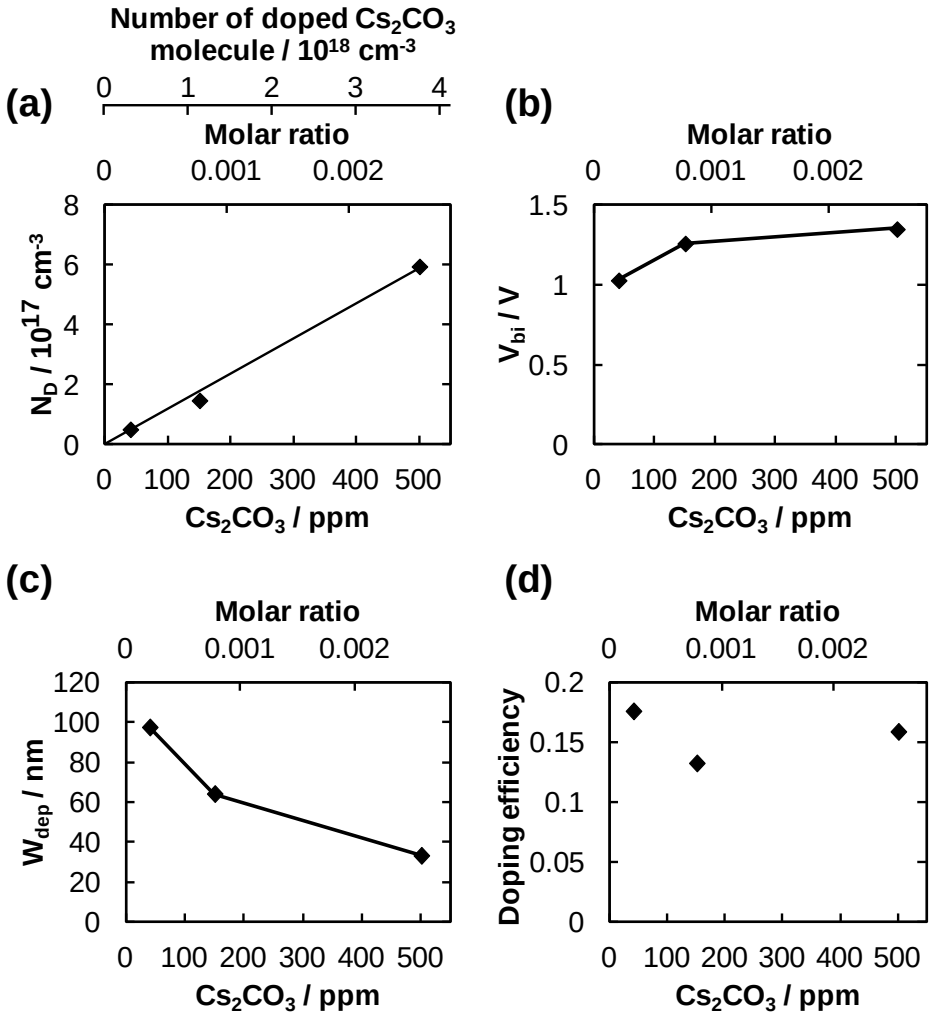

Fig. 5.3 Dependences of donor concentration (N_D) (a), built-in potential (V_{bi}) (b), depletion layer width (W_{dep}) (c), and doping efficiency (d) on the Cs_2CO_3 doping concentrations in a given volume. The number of doped Cs_2CO_3 molecules per unit volume is also shown on the upper horizontal axis of Fig. 5.3(a). Molar ratio, i.e., the ratio of the number of Cs_2CO_3 molecules to that of the sum of the C_{60} and 6T molecules, is also shown on the upper horizontal axis.

Figs. 5.3(a)–5.3(c) show the relationship between the obtained Schottky junction parameters, i.e., N_D, V_{bi}, and W_{dep}, and the concentration of Cs_2CO_3. The proportional relationship between the doping concentration and the value of N_D (**Fig. 5.3(a)**) proves that Cs_2CO_3 acts as a donor dopant, since N_D represents the number of positive charges of a spatially fixed ionized donor ($Cs_2CO_3^+$), namely, the space charges in the depletion layer. At 500 ppm, the value of N_D reached 6 x 10^{17} cm^{-3}. On the other hand, V_{bi} showed a constant value of around 1.2 eV, which is far smaller than the difference in Fermi levels (2.2 eV) between MoO_3 (6.7 eV) and a Cs_2CO_3-doped (500 ppm) C_{60}:6T film (4.5 eV).

Fig. 5.4 shows the energy band diagrams of the *n*-type Schottky junctions for each of the doping concentrations. The obtained values of W_{dep} are very small, and shrink with increasing doping concentration, i.e., 97, 64, and 33 nm for 40, 150, and 500 ppm doping, respectively. The reductions in photocurrent and EQE at the highest concentration of 500 ppm (**Figs. 5.1(b)** and **5.1(c)**) can be reasonably explained by a diminished photoactive region due to the extremely thin W_{dep} (33 nm) compared with the deep penetration depth of the irradiated light, e.g., 90% of the incident light is absorbed within 100 nm at a wavelength of 380 nm. On the other hand, the observed improvement in the rectification behavior and the increase in the fill factor (**Fig. 5.1(c)**) are obviously due to the decrease in cell resistance caused by the increase in N_D (**Fig. 5.3(a)**).

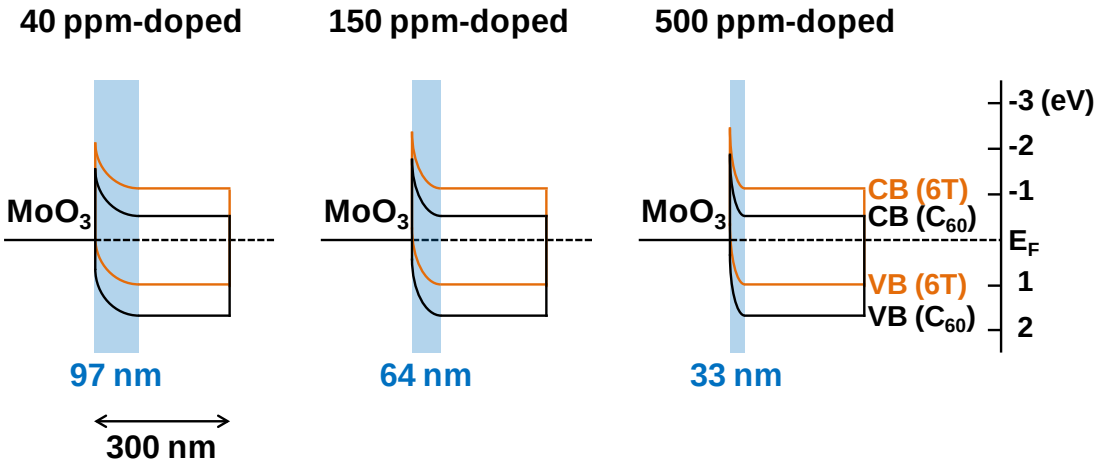

Fig. 5.4 Energy-band diagrams of the Cs_2CO_3-doped C_{60}:6T cells based on the obtained barrier parameters. C_{60} and 6T are shown by the black and orange curves, respectively. The blue shaded areas indicate the depletion layers. CB and VB denote the conduction band and valence band, respectively.

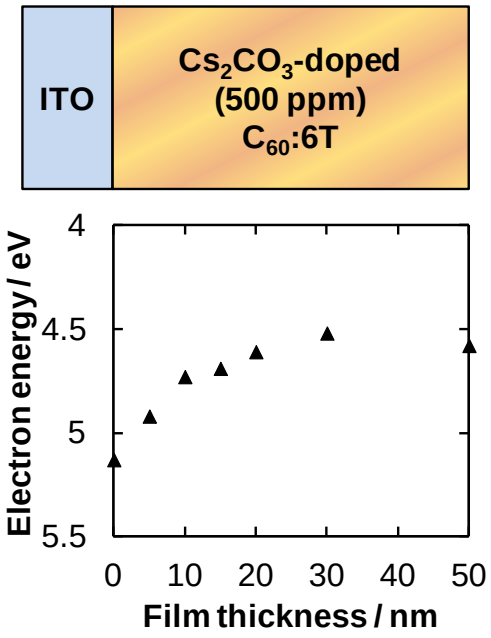

Fig. 5.5 Dependence of value of E_F on the thickness of 500 ppm Cs_2CO_3 doped C_{60}:6T films deposited on ITO.

In order to cross-check the barrier parameters obtained from the capacitance measurements (**Figs. 5.3** and **5.4**), the author measured the position of E_F by changing the film thicknesses of a 500 ppm Cs_2CO_3-doped C_{60}:6T film on an O_2-plasma treated ITO electrode (work function: 5.13 eV) by using a Kelvin probe (**Fig. 5.5**).[14,17] Between 0 nm and 20 nm, E_F gradually shifted negatively, i.e., E_F gradually approached the conduction band of 6T:C_{60}. Above 20 nm, E_F became constant. The values of E_F for 6T:C_{60} thicknesses of 0 nm and 20 nm correspond to those of ITO (5.13 eV) and 500 ppm Cs_2CO_3-doped C_{60}:6T (4.52 eV), respectively. Band bending of the Schottky junction formed at the ITO/Cs_2CO_3-doped C_{60}:6T interface is just an 'upside-down' version of the curve shown in **Fig. 5.5**. From this curve, the author can determine that the values of N_D, W_{dep}, and V_{bi} are 7 x 10^{17} cm^{-3}, 20 nm, and 0.6 V, respectively. For C_{60}:6T films doped with the same concentration of Cs_2CO_3 (500 ppm), the same carrier concentration (N_D) should be obtained, irrespective of the interfaces with MoO_3 and ITO.[24] Actually, the N_D values obtained by the capacitance measurement for the MoO_3/C_{60}:6T interface (6 x 10^{17} cm^{-3}) and that obtained by the Kelvin measurement for the ITO/C_{60}:6T interface (7 x 10^{17} cm^{-3}) coincide well. This provides quantitative support for the parameters observed in **Fig. 5.3**.

The doping efficiency, which is defined as the ratio of the number of doping-induced electrons (N_D) to the number of doped Cs_2CO_3 molecules per unit volume (cm^{-3}), was calculated to be around 0.15 (**Fig. 5.3(d)**). The doping efficiency is expressed by the multiplication of two factors, i.e., the formation efficiency of a charge-transfer (CT) complex, i.e., C_{60}^----$Cs_2CO_3^+$ and $6T^-$---$Cs_2CO_3^+$, and the ionization efficiency, i.e., the rate of liberation of negative charges from the positive charges on the ionized donor ($Cs_2CO_3^+$). Since Cs_2CO_3 is a substantial molecule with

the structure [CsO-C(=O)-OCs] and there is no sign of dissociation during vacuum deposition, it is reasonable to assume that most of the Cs_2CO_3 is doped as a single molecule and forms a CT complex with C_{60} under the present low-doping concentration. Therefore, the author believes that the ionization efficiency of the CT complex is around 15%, which seems a significantly large value, although it is still smaller than the ionization efficiency of 100% that is observed when P is used as a dopant in Si.

5.4. Conclusion

In this chapter, it was confirmed that the junction parameters of *n*-type Schottky junctions formed at MoO_3/C_{60}:6T interfaces could be tuned by ppm-level doping with Cs_2CO_3. The present results strongly support the theory that Cs_2CO_3 acts as a donor dopant for C_{60}:6T co-deposited films.

5.5. References

1) Organic photovoltaics, Mechanisms, Materials and Devices, edited by S.–S. Sun and N. S. Sariciftci, published by CRC Press, New York, March (2005).
2) H. Spanggaard and F. C. Krebs, *Sol. Energy Mater. Sol. Cells*, **83**, 125 (2004).
3) H. Hoppe and N. S. Sariciftci, *J. Mater. Res*., **19**, 1924 (2004).
4) C. W. Tang, *Appl. Phys. Lett.*, **48**, 183 (1986).
5) M. Hiramoto, H. Fujiwara, and M. Yokoyama, *Appl. Phys. Lett.*, **58**, 1062 (1991).
6) M. Hiramoto and K. Sakai, *Mol. Cryst. Liq. Cryst*., **491**, 284 (2008).
7) T. Kaji, M. Zhang, S. Nakao, K. Iketaki, K. Yokoyama, C. W. Tang, and M. Hiramoto, *Adv. Mater.*, **23**, 3320 (2011).
8) M. Riede, C. Uhrich, J. Widmer, R. Timmreck, D. Wynands, G. Schwartz, W.-M. Gnehr, D. Hildebrandt, A. Weiss, J. Hwang, S. Sundarraj, P. Erk, M. Pfeiffer, and Karl Leo, *Adv*. *Funct*. *Mater*., **21**, 3019 (2011).
9) W. E. Spear and P. E. Lecomber, *Solid State Commun.*, **17**, 1193 (1975).
10) M. Kubo, K. Iketaki, T. Kaji, and M. Hiramoto, *Appl. Phys. Lett.*, **98**, 073311 (2011).
11) M. Kubo, T. Kaji, and M. Hiramoto, *AIP Advances*, **1**, 032177 (2011).
12) Y. Shinmura, M. Kubo, N. Ishiyama, T. Kaji, and M. Hiramoto, *AIP Advances*, **2**, 032145 (2012).
13) J. Sakai, T. Taima, and K. Saito, *Organic Electronics*, **9**, 582 (2008).
14) N. Ishiyama, M. Kubo, T. Kaji, and M. Hiramoto, *Appl. Phys. Lett.*, **99**, 133301 (2011).
15) H.–H. Liao, L.–M. Chen, Z. Xu, G. Li, and Y. Yang, *Appl. Phys. Lett.*, **92** 173303 (2008).

16) S. Hamwi, T. Riedl, and W. Kowalsky, *Appl*. *Phys*. *Lett*., **99**, 053301 (2011).

17) N. Ishiyama, M. Kubo, T. Kaji, and M. Hiramoto, *Appl*. *Phys*. *Lett*., **101**, 233303 (2012).

18) A. J. Twarowski and A. C. Albrecht, *J*. *Chem*. *Phys*., **70**, 2255 (1979).

19) M. Tomida, S. Kusabayashi, and M. Yokoyama, *Chem*. *Lett*., **8**, 1305 (1984).

20) R. A. Laudise, Ch. Kloc, P. G. Simpkins, and T. Siegrist, *J*. *Crystal Growth*, **187**, 449 (1998).

21) Under irradiation onto the Ag electrode, the photocurrent appeared in the weak absorption region (500-700 nm) of the cell due to the masking effect. This offers additional strong evidence that the photoactive interface is that between MoO_3/C_{60}:6T.

22) C_{60} and 6T form CT complexes with Cs_2CO_3, i.e., C_{60}^----$Cs_2CO_3^+$ and $6T^-$---$Cs_2CO_3^+$, which were confirmed to form by the appearance of CT absorption. Here, the positive charge on the $Cs_2CO_3^+$ group can be regarded as a spatially fixed positive ion, i.e., an ionized donor. The negative charges on C_{60} and 6T can be liberated by thermal energy and can act as free electrons in the conduction band. So, Cs_2CO_3 acts as a donor dopant and renders C_{60}:6T *n*-type.

23) A. F. Hebard, R. C. Hadon, R. M. Fleming, and A. R. Kortan, *Appl*. *Phys*. *Lett*., **59**, 2109 (1991).

24) In the cases of W_{dep} and V_{bi}, different values should be observed for the different interfaces of MoO_3/C_{60}:6T and ITO/C_{60}:6T.

Chapter 6:

Doping-based Design of Organic Solar Cells in Co-deposited Films

"Tandem organic solar cells formed in co-deposited films by doping", Norihiro Ishiyama, Masayuki Kubo, Toshihiko Kaji, and Masahiro Hiramoto, submitted.

Abstract

Tandem organic solar cells, in which two single p^+in^+-homojunctions are connected by a heavily-doped n^+p^+-ohmic interlayer, were formed in co-deposited films consisting of fullerene and α-sexithiophene simply by doping with molybdenum oxide and cesium carbonate. The single and tandem cells showed open-circuit voltages of 0.85V and 1.69 V and conversion efficiencies of 1.6% and 2.4%, respectively.

6.1. Introduction

For small-molecular-type organic photovoltaic cells,[1-7] doping-based control of the energy structure[8-11] is a significant challenge to creating a built-in potential, as is the case with inorganic cells.[12] For fullerene (C_{60}) single films, the author has reported the realization of complete *pn*-control[13] and the formation of a *pn*-homojunction[14] and a tandem cell[15,16] consisting of two single *pn*-homojunction cells connected by a heavily-doped n^+p^+-tunneling junction.[17]

On the other hand, co-deposited films consisting of two kinds of organic semiconductors are essential in order to generate photocurrent densities of significant magnitude based on the dissociation of excitons by the photoinduced electron transfer process.[1-7] The author believes that the formation of a built-in potential by direct-doping in the bulk of co-deposited films, where the generation and transport of photocarriers occurs, has the potential to enhance the efficiency of these cells. Moreover, in this type of cells, short exciton diffusion length is no longer a limitation factor of cell performance. In **chapters 4** and **5**, the author succeeded in achieving complete *pn*-control of co-deposited films consisting of C_{60} and α-sexithiophene (C_{60}:6T).[18,19] Thus, as a next step, the author attempted to incorporate p^+in^+-homojunctions and their corresponding tandem cells in C_{60}:6T co-deposited films by doping only. Here, the symbol plus (+) in p^+ and n^+ indicates heavy doping. Molybdenum oxide (MoO_3)[13,14,17,18] and cesium carbonate (Cs_2CO_3)[11,17,19-21] were used as acceptor and donor dopants, respectively.

In this chapter, the author describes p^+in^+-homojunctions and their corresponding tandem cells formed directly in the bulk of photovoltaic C_{60}:6T co-deposited films by doping only.

6.2. Experimental

C_{60} (Frontier Carbon, nanom purple TL) and 6T (Tokyo Chemical Industry) samples purified by single-crystal sublimation[6,22] under flowing N_2 at 1 atm and 0.1 atm, respectively, were used. MoO_3 (Alfa Aeser, 99.9995%) and Cs_2CO_3 (Sigma-Aldrich, 99.995%) were used without further purification for the acceptor and donor dopants, respectively. **Figs. 6.1(a)** and **6.1(b)** show the structures of a single p^+in^+-homojunction cell and a tandem cell connecting two p^+in^+-homojunctions formed in C_{60}:6T co-deposited films. The C_{60}:6T film was vacuum deposited on an indium tin oxide (ITO) substrate, which was not exposed to an oxygen plasma, at 10^{-4} Pa in an oil-free vacuum evaporator (EpiTech Inc., ET300-6E-HK). The ratio of C_{60}:6T was maintained at 10:1.[23] Doping was performed with MoO_3 and Cs_2CO_3 using a 'three component co-evaporation' technique.[18] Ohmic contacts to the ITO and Ag electrodes were formed by inserting heavily-doped 10 nm-thick p^+ and n^+ layers adjacent to the electrodes.[17,21] The doping concentrations of MoO_3 for the p^+ contact and Cs_2CO_3 for the n^+ contact were 50,000 ppm and 10,000 ppm by volume, respectively. To fabricate the tandem cell, an n^+p^+-homojunction interlayer was formed between two unit cells (Fig. 6.1(b)). The doping concentrations of both Cs_2CO_3 for the n^+-layer and MoO_3 for the p^+-layer were 50,000 ppm. Measurements of the cells were performed at 10^{-3} Pa. The Fermi levels (E_F) of the C_{60}:6T films were measured using a Kelvin vibrating capacitor apparatus (Riken-Keiki, FAC-1) without exposure to air at any time.

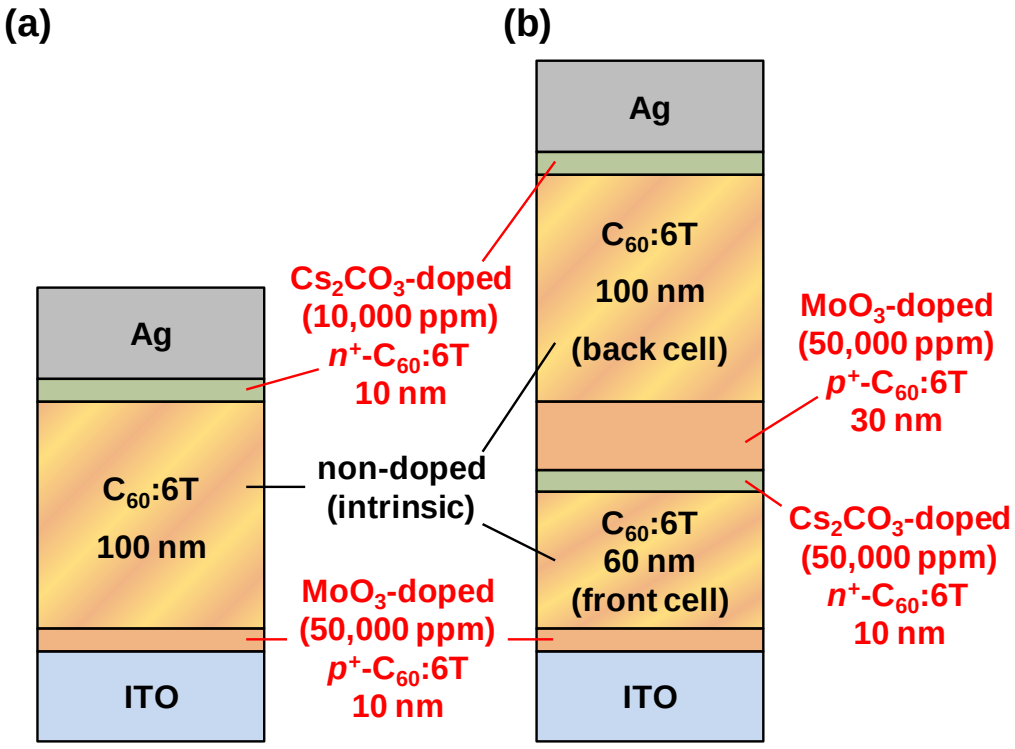

Fig. 6.1 (a) Structure of a p^+in^+-homojunction cell fabricated in a C_{60}:6T co-deposited film. A non-doped intrinsic C_{60}:6T layer is sandwiched between heavily doped p^+ and n^+-C_{60}:6T layers. (b) Structure of a tandem cell connecting two unit p^+in^+-homojunction cells.

6.3. Results and Discussion

6.3.1. Design of p^+in^+-C_{60}:6T Homojunction Cells

Fig. 6.2 shows the current-voltage (*J*-*V*) characteristics of the cells shown in **Fig. 6.1**. Both cells showed photovoltages indicating that ITO is positive and Ag is negative. A single p^+in^+-homojunction cell (blue curves A) (**Fig. 6.1(a)**) showed the following cell parameters; a short-circuit photocurrent (J_{sc}) of 4.5 mA cm^{-2}, an open-circuit photovoltage (V_{oc}) of 0.85 V, a fill factor (FF) of 0.41, and a conversion efficiency of 1.6%. **Fig. 6.3(a)** (blue curve A) shows the action spectrum of the external quantum efficiency (EQE) of J_{sc} for the single cell (**Fig. 6.1(a)**). The photocurrent response appeared throughout the wavelength region, from 300 nm to 700 nm. Taking the shape of the absorption spectrum of a single C_{60}:6T cell (**Fig. 6.3(a)**, black curve) into consideration, the photocurrent is generated equally, irrespective of the light penetration depth, i.e., the strong absorption region (300-500 nm) where light is absorbed near the ITO electrode and the weak absorption region (500-700 nm) where a significant amount of the light is transmitted near to the Ag electrode. This suggests that the photocurrent is uniformly generated across the non-doped C_{60}:6T co-deposited film. In order to confirm this, the author fabricated an inverted version of the cell shown in **Fig. 6.1(a)**, i.e., an ITO/n^+-C_{60}:6T(10 nm)/C_{60}:6T(100 nm)/p^+-C_{60}:6T(10 nm)/Ag cell. Under light irradiation to the ITO electrode, almost the same *J*-*V* curve as in **Fig. 6.2** (blue curve A) and almost the same shape and magnitude of action spectrum (**Fig. 6.3(a)**, orange curve B) as in **Fig. 6.3(a)** (blue curve A) were observed. The same EQE spectra for the photocurrent, irrespective of the side onto which light was irradiated, clearly tells us that the built-in potential in the present cell is symmetrical and that a uniform electric field is formed across the non-doped C_{60}:6T

co-deposited film, which acts as an intrinsic layer. Thus, single p^+in^+-homojunction cells were successfully fabricated in C_{60}:6T co-deposited films by doping only.

6.3.2. Design of a Tandem C_{60}:6T Solar Cell

As a next step, the author fabricated a tandem cell (**Fig. 6.1(b)**) by connecting two unit p^+in^+-homojunction cells. The following cell parameters were obtained; J_{sc} of 3.0 mA cm^{-2}, V_{oc} of 1.69 V, FF of 0.47, and a conversion efficiency of 2.4% (**Fig. 6.2**, red curves B). Compared with the single cell (**Fig. 6.2**, blue curves A), V_{oc} has doubled from 0.85 V to 1.69 V. Obviously, the n^+p^+-homojunction in **Fig. 6.1(b)** acts as an ohmic interlayer to connect the unit cells. On the other hand, the author calculated the action spectrum of EQE for the 'back cell' incorporated in the tandem cell (**Fig. 6.3(b)**, broken curve B) by multiplying the EQE value of the single cell (**Fig. 6.3(a)**, blue curve A) and the transmittance of the front cell for each wavelength. Clear coincidence between the observed and calculated spectra is confirmed (**Fig. 6.3(b)**). For the present tandem cell, the magnitude of the photocurrent is dominated by the back cell operating under the light attenuated by the front cell. Based on the above observations, the author concluded that a tandem cell was successfully formed in C_{60}:6T co-deposited films by only doping with Cs_2CO_3 and MoO_3.

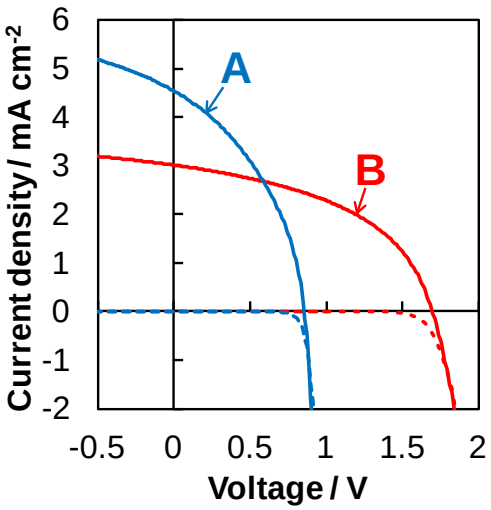

Fig. 6.2 Current voltage (*J*-*V*) characteristics for a single p^+in^+-homojunction cell (blue curves A)(Fig. 6.1(a)) and a tandem cell (red curves B)(Fig. 6.1(b)). The photo and dark currents are shown by the solid and the broken curves, respectively. The ITO electrode was irradiated with simulated solar light (AM 1.5, 100 mW cm^{-2}). The cell parameters, i.e., J_{sc}, V_{oc}, FF, and efficiency. Curve A: 4.5 mA cm^{-2}, 0.85 V, 0.41, 1.6%. Curve B: 3.0 mA cm^{-2}, 1.69 V, 0.47, 2.4%.

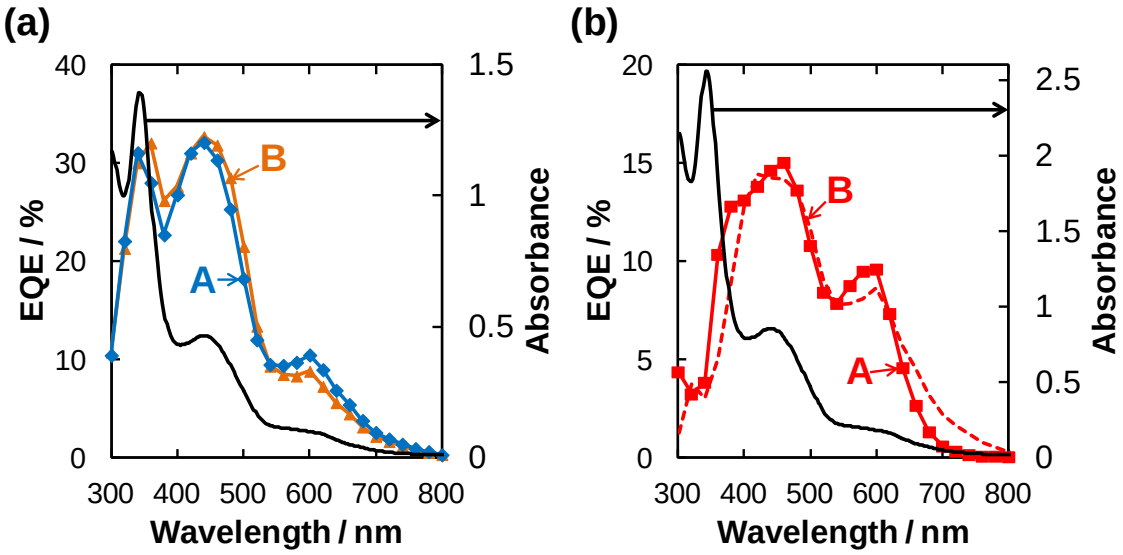

Fig. 6.3 (a) Action spectra of external quantum efficiency (EQE) for the single p^+in^+-homojunction cell shown in Fig. 6.1(a) (blue curve A) and for an inverted cell with the structure of ITO/n^+-C_{60}:6T/C_{60}:6T/p^+-C_{60}:6T/Ag (orange curve B). The black curve shows the absorption spectrum of a C_{60}:6T film having the same thickness as the cell shown in Fig. 6.1(a) (120 nm). (b) Action spectrum of EQE (solid curve A) for the tandem cell (Fig. 6.1 (b)) and calculated spectrum (broken curve B). The black curve shows the absorption spectrum of a C_{60}:6T film having the same thickness as the cell shown in Fig. 6.1(b) (220 nm).

6.3.3. Energy Band Diagram of a Tandem C_{60}:6T Solar Cell

In order to illustrate the whole energy structure of the tandem cell, energy-band mapping of p^+in^+- and n^+p^+-homojunctions was performed using a Kelvin probe.[17,18,24] The positions of the Fermi levels (E_F) for different C_{60}:6T thicknesses near the homojunction were measured. To illustrate the presence of a p^+in^+-homojunction, E_F values for non-doped C_{60}:6T films on doped films were measured (blue curves A in **Figs. 6.4(a)** and **6.4(b)**). E_F hardly changed and maintained almost constant values on both the MoO_3-doped film (**Fig. 6.4(a)**) and on the Cs_2CO_3-doped (**Fig. 6.4(b)**). These constant E_F values indicate that the non-doped C_{60}:6T films act as insulators. As a result, when a unit cell having the structure of MoO_3-doped (50,000 ppm)/non-doped/Cs_2CO_3-doped (50,000 ppm), i.e., a p^+/insulator/n^+, is fabricated, the built-in electric field generated by the differences in E_F between the MoO_3 and Cs_2CO_3 doped layers (5.6 - 4.4 = 1.2 eV) (see **Figs. 6.4(a)** and **6.4(b)**, C_{60}:6T thickness = 0 nm) are uniformly distributed across the insulating non-doped C_{60}:6T film. Thus, two p^+in^+-homojunctions can be depicted in the front and back cells (**Fig. 6.5**).

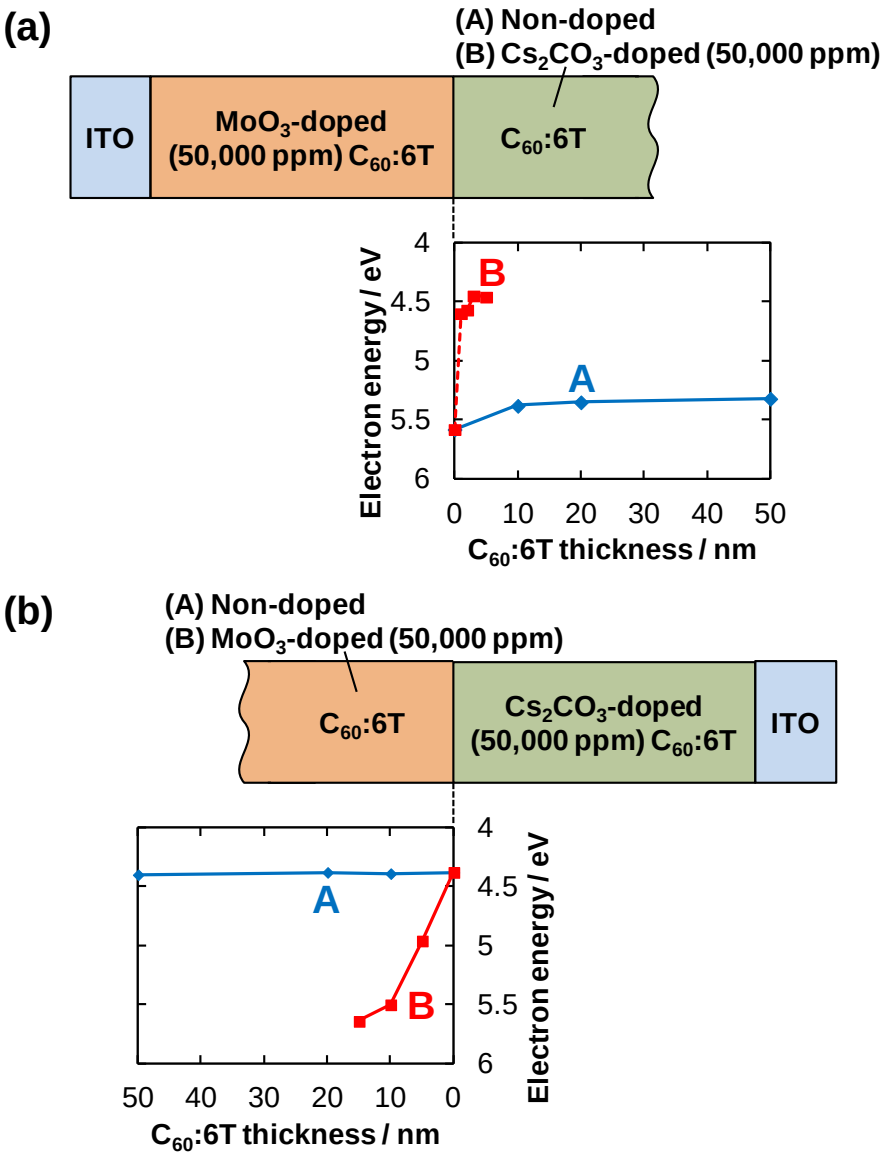

Fig. 6.4 Energy level mapping of homojunctions using a Kelvin probe. The sample structures and the dependence of the position of the Fermi level (E_F) on the thicknesses of non-doped or doped C_{60}:6T films are shown. (a) Non-doped (blue curve A) or Cs_2CO_3-doped (red curve B) deposited on a MoO_3-doped C_{60}:6T film. (b) Non-doped (blue curve A) or MoO_3-doped (red curve B) C_{60}:6T film deposited on a Cs_2CO_3-doped C_{60}:6T film.

To illustrate the presence of an n^+p^+-homojunction, E_F values for Cs_2CO_3-doped films on the MoO_3-doped films (red curve B in **Fig. 6.4(a)**) and those for MoO_3-doped films on Cs_2CO_3-doped films (red curve B in **Fig. 6.4(b)**) were measured. All doping concentrations of MoO_3 and Cs_2CO_3 are 50,000 ppm. In the former case, a rapid negative shift in E_F ended within 3 nm and reached the original E_F position of Cs_2CO_3-doped C_{60}:6T (4.38 eV, see **Fig. 6.4(b)**, C_{60}:6T thickness = 0 nm). In the latter case, a quick positive shift in E_F ended within 15 nm and reached the original E_F position of MoO_3-doped C_{60}:6T (5.58 eV, see **Fig. 6.4(a)**, C_{60}:6T thickness = 0 nm). Based on these complementary observations, the potential profile of the depletion layer of an n^+p^+-homojunction (**Fig. 6.5**, red shaded region, width: 18 nm) can be drawn.

The overall energy band diagram of a tandem cell is shown in **Fig. 6.5**. Under light irradiation, electrons and holes are photo-generated in both the front and back cells. Electrons and holes that move toward the n^+p^+-ohmic interlayer neutralize each other due to recombination or tunneling. This process is consistent with the observed photovoltaic properties of the present tandem cell (**Figs. 6.2** and **6.3**).

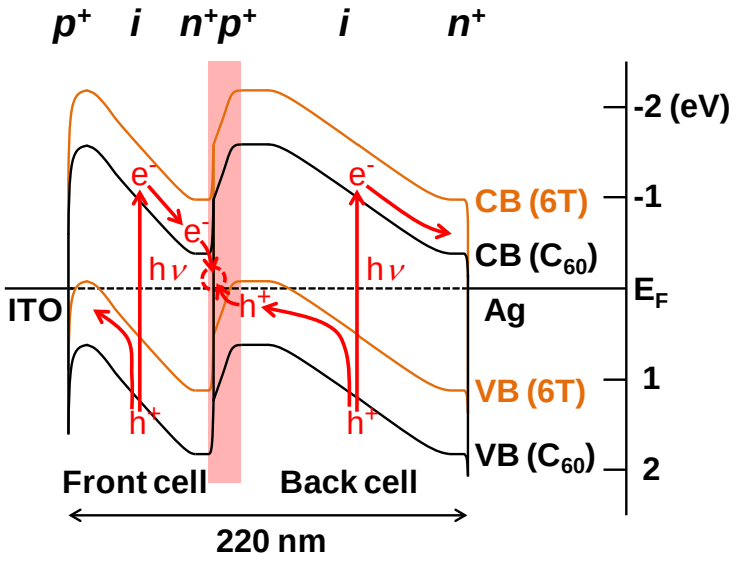

Fig.6.5 Energy band diagram of a tandem cell based on Kelvin probe measurements (Fig. 6.4). The red shaded region corresponds to the depletion layer for an n^+p^+-homojunction acting as an ohmic interlayer. VB and CB denote the valence band and the conduction band, respectively. The bands for C_{60} and 6T are shown by the black and orange curves, respectively.

6.4. Conclusion

In this chapter, p^+in^+-homojunctions and corresponding tandem cells were successfully fabricated in C_{60}:6T co-deposited films by doping with MoO_3 and Cs_2CO_3. The heavily-doped n^+p^+-homojunction was confirmed to act as an ohmic interlayer. For the tandem cell, a large V_{oc} value of 1.69 V and an efficiency of 2.4% were obtained.

6.5. References

1) Organic photovoltaics, Mechanisms, Materials and Devices, edited by S. –S. Sun and N. S. Sariciftci, published by CRC Press, New York, March (2005).

2) H. Spanggaard and F. C. Krebs, *Sol. Energy Mater. Sol. Cells*, **83**, 125 (2004).

3) H. Hoppe and N. S. Sariciftci, *J. Mater. Res*., **19**, 1924 (2004).

4) C. W. Tang, *Appl. Phys. Lett.*, **48**, 183 (1986).

5) M. Hiramoto, H. Fujiwara, and M. Yokoyama, *Appl. Phys. Lett.*, **58**, 1062 (1991).

6) M. Hiramoto and K. Sakai, *Mol. Cryst. Liq. Cryst*., **491**, 284 (2008).

7) T. Kaji, M. Zhang, S. Nakao, K. Iketaki, K. Yokoyama, C. W. Tang, and M. Hiramoto, *Adv. Mater.*, **23**, 3320 (2011).

8) K. Walzer, B. Maennig, M. Pfeiffer, and K. Leo, *Chem. Rev.*, **107**, 1233 (2007).

9) G. Li, R. Zhu, and Y. Yang, *Nature Photon*., **6**, 153 (2012).

10) M. Hiramoto, K. Ihara, and M. Yokoyama, *Jpn. J. Appl. Phys*., **34**, 3803 (1995).

11) S. Hamwi, T. Riedl, W. Kowalsky, *Appl. Phys. Lett.*, **99**, 053301 (2011).

12) W. E. Spear and P. E. Lecomber, *Solid State Commun.*, **17**, 1193 (1975).

13) M. Kubo, K. Iketaki, T. Kaji, and M. Hiramoto, *Appl. Phys. Lett.*, **98**, 073311 (2011).

14) M. Kubo, T. Kaji, and M. Hiramoto, *AIP Advances*, **1**, 032177 (2011).

15) M. Hiramoto, M. Suezaki, and M. Yokoyama, *Chem. Lett.*, **19**, 327 (1990).

16) T. Ameri, G. Dennler, C. Lungenschmied and C. J. Brabec, *Energy Environ. Sci*., **2**, 347 (2009).

17) N. Ishiyama, M. Kubo, T. Kaji, M. Hiramoto, *Appl. Phys. Lett*, **101**, 233303 (2012).

18) N. Ishiyama, M. Kubo, T. Kaji, and M. Hiramoto, *Appl. Phys. Lett.*, **99**, 133301

(2011).

19) N. Ishiyama, T. Yoshioka, T. Kaji, and M. Hiramoto, *Appl. Phys. Express*, **6**, 012301 (2013).

20) H.–H. Liao, L.–M. Chen, Z. Xu, G. Li, and Y. Yang, *Appl. Phys. Lett.*, **92** 173303 (2008).

21) M. Kubo, Y. Shinmura, N. Ishiyama, T. Kaji, and M. Hiramoto, *Appl. Phys. Express*, **5**, 092302 (2012).

22) R. A. Laudise, Ch. Kloc, P. G. Simpkins, and T. Siegrist, *J. Cyrstal Growth*, **187**, 449 (1998).

23) J. Sakai, T. Taima, and K. Saito, *Org. Electron*., **9**, 582 (2008).

24) N. Hayashi, H. Ishii, Y. Ouchi, and K. Seki, *J. Appl. Phys*., **92**, 3784 (2002).

Chapter 7:

General Conclusion

7.1. Summary of this Thesis

In this thesis, the author constructed doping techniques for designing the energy structures of photovoltaic organic co-deposited films, as follows.

(i) The complete control of *pn*-properties of photovoltaic co-deposited films consisting of fullerene and α-sexithiophene (C_{60}:6T) was demonstrated by doping with molybdenum oxide (MoO_3) and (Cs_2CO_3) (**Fig. 7.1**).

(ii) A series of fundamental junctions, that is, *p*- and *n*-type Schottky junctions (**Fig. 7.2**), *pn*, p^+in^+, and ohmic n^+p^+ homojunctions (**Fig. 7.3**), and ohmic contacts between metal electrodes and heavily-doped p^+ and n^+ layers were fabricated in the C_{60}:6T films by precise control of the MoO_3 and Cs_2CO_3 doping.

(iii) A 2.4% efficient tandem organic solar cell was formed by connecting two photoactive p^+in^+- homojunctions with an n^+p^+-ohmic interlayer (**Fig. 7.4**).

Doping into a C_{60}:6T co-deposited film was achieved by the use of a 'three component co-evaporation' technique. Precise monitoring of the deposition rates of the dopants using a computer monitoring system enabled us to dope as low as 40 ppm by volume concentration. Energy-band mapping using a Kelvin probe and capacitance measurements assisted in the clarification of the operating mechanism of the doped junctions.

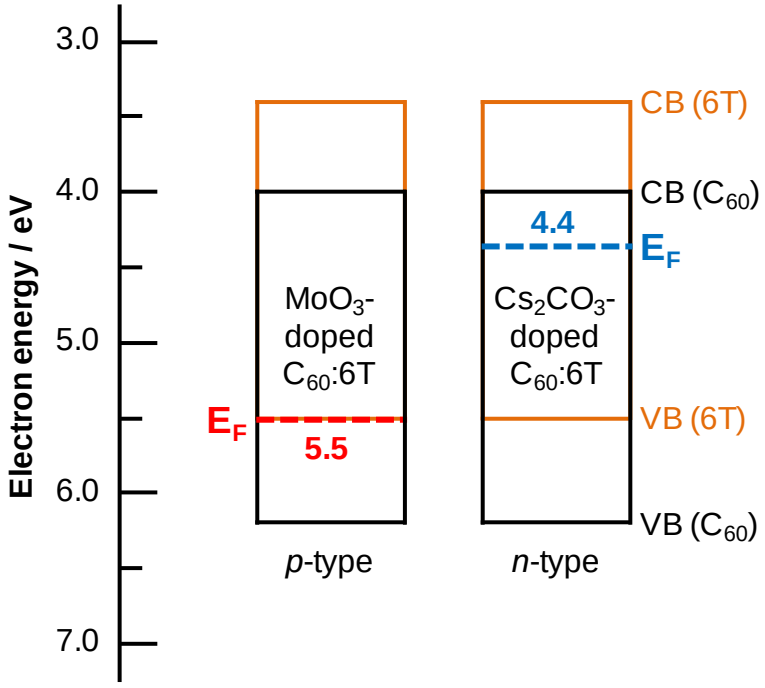

Fig. 7.1 Energy diagram of C_{60}:6T co-deposited films doped with MoO_3 and Cs_2CO_3.

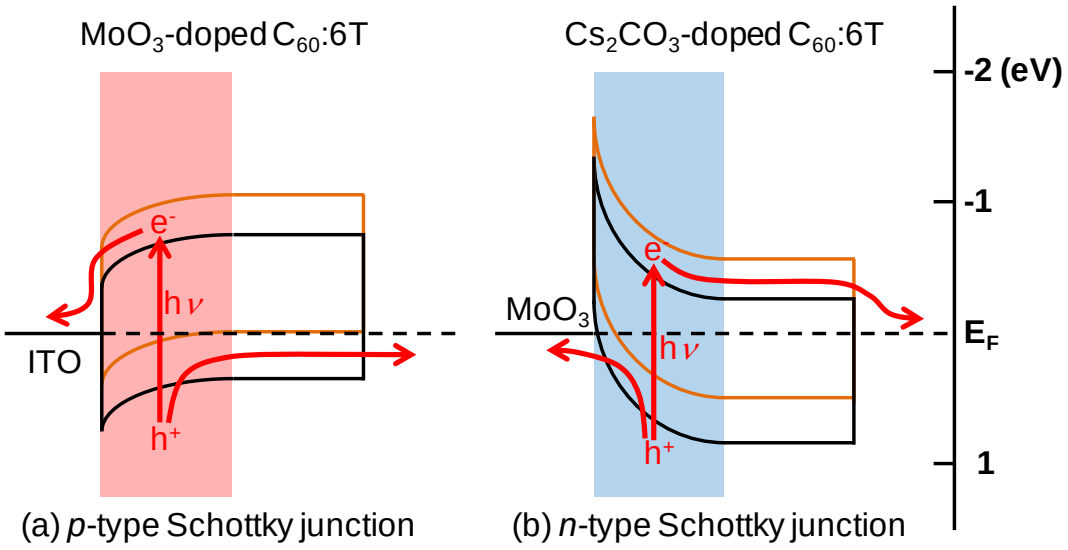

Fig. 7.2 Energy-band diagrams of Schottky junctions in C_{60}:6T films.

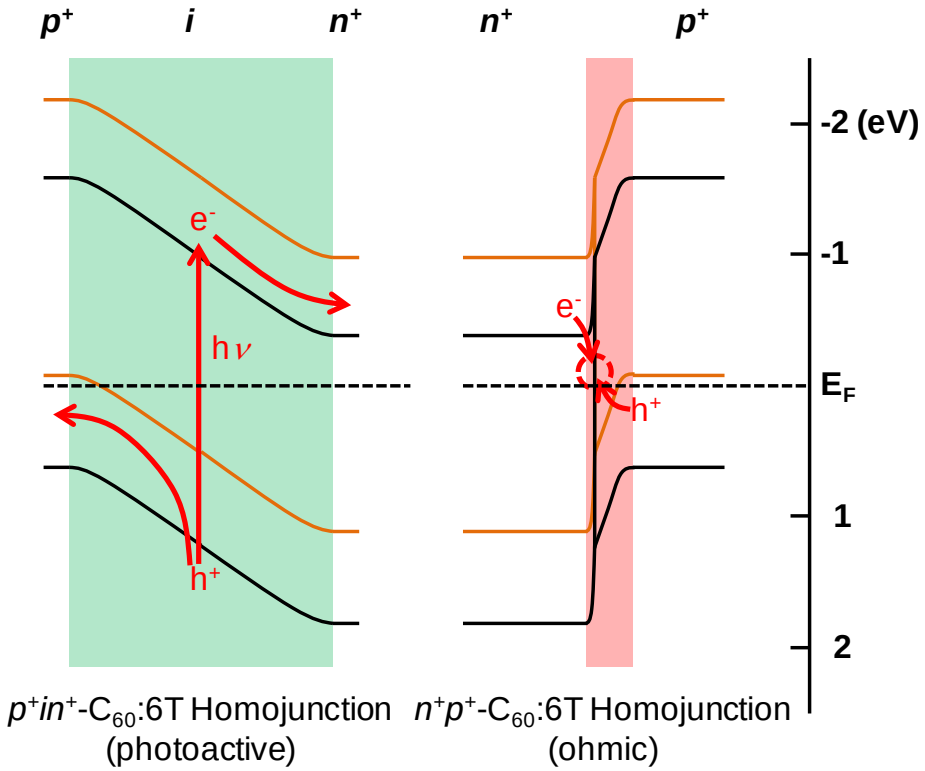

Fig. 7.3 Energy-band diagrams of p^+in^+ and n^+p^+ homojunctions in C_{60}:6T films.

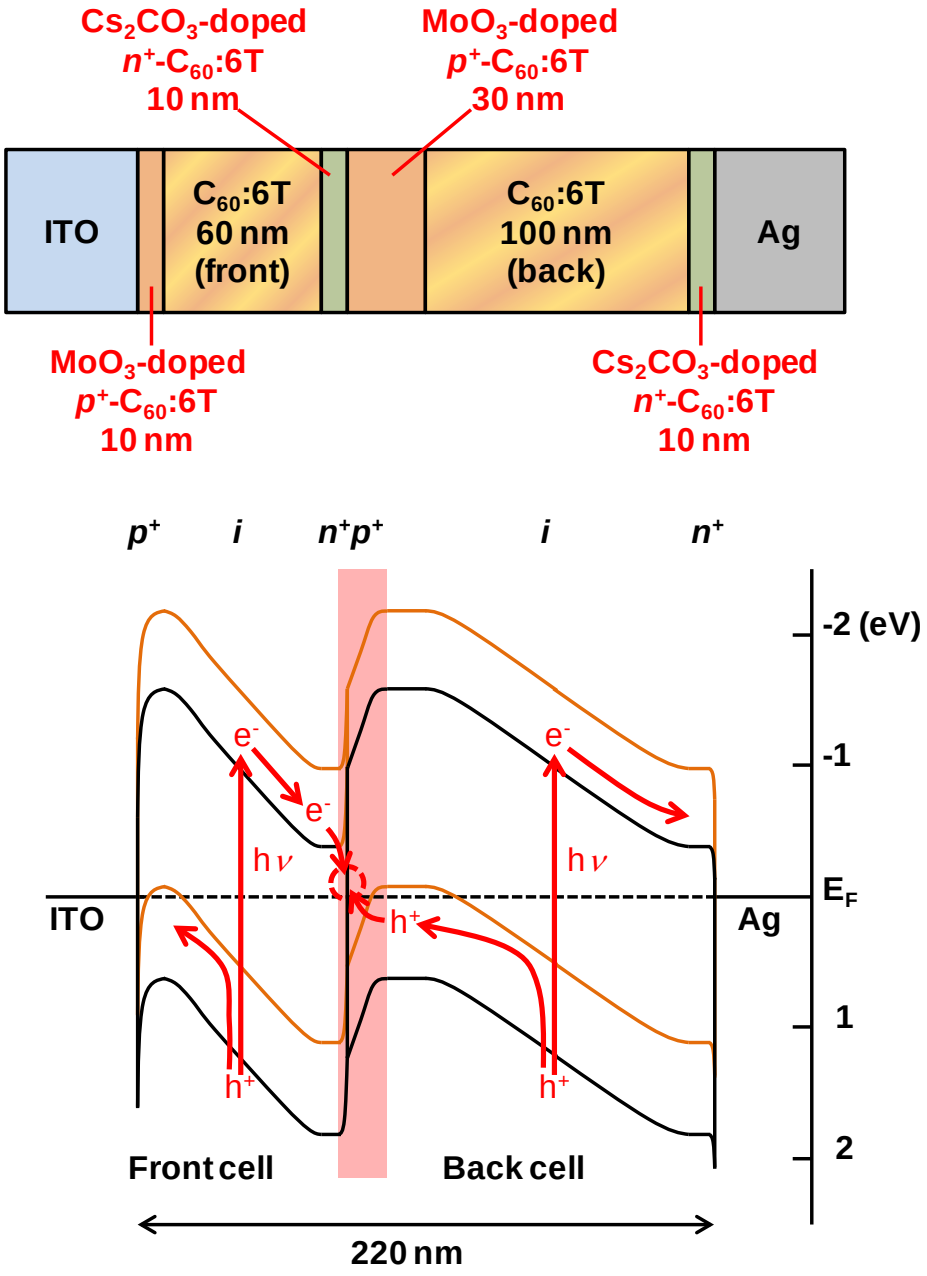

Fig. 7.4 Structure of a tandem solar cell formed in a C_{60}:6T film and energy-band diagram of the overall cell.

pn-homojunctions and an n^+p^+-homojunction, which act as photoactive layers

and as an ohmic interlayer, respectively, were fabricated in single C_{60} films by simply controlling the doping concentrations of MoO_3 and Cs_2CO_3. A tandem photovoltaic cell, whose open circuit voltage (V_{oc}) is double that of the unit cells, was incorporated into single C_{60} films by doping alone. The energy-band diagram of the overall tandem cell was depicted based on Kelvin probe measurements for the *pn*- and n^+p^+homojunctions. The *pn*-homojunctions, in which an exciton is dissociated into a hole and an electron under photo-irradiation, have 130 nm-wide depletion layers. The n^+p^+-homojunction, in which a hole and an electron neutralize each other due to recombination or tunneling, has a 20 nm-wide depletion layer. A doping technique for controlling the energy structures of single C_{60} films was established.

Control of the energy structure of a C_{60}:6T co-deposited film was achieved by ppm-level doping with MoO_3. The conduction types of C_{60}:6T films were intentionally tuned from *n*-type, via intrinsic, to *p*-type (**Fig. 7.2(a)**) by controlling the MoO_3 doping concentration. Mapping of the potential profiles of MoO_3-doped C_{60}:6T films using a Kelvin probe enabled us to confirm the transition of the energy structure. The results confirmed that MoO_3 acts as an acceptor dopant in the case of C_{60}:6T co-deposited films.

Tuning of the barrier parameters of *n*-type Schottky junctions formed in C_{60}:6T co-deposited films (**Fig. 7.2(b)**) was achieved by ppm-level control of Cs_2CO_3 doping. The carrier concentration of electrons, as evaluated by capacitance measurements, showed a clear proportional relationship to the doping concentration of Cs_2CO_3. The results confirmed that Cs_2CO_3 acts as a donor dopant for the C_{60}:6T co-deposited films. In addition, the doping efficiency was found to be around 0.15.

Since the *pn*-properties of the C_{60}:6T co-deposited films could be completely

controlled by doping with MoO_3 and Cs_2CO_3 (**Fig. 7.1**), organic solar cells were designed in the C_{60}:6T films by using these doping techniques. The author fabricated a series of fundamental junctions; that is, *p*- and *n*-type Schottky junctions (**Fig. 7.2**); *pn*, p^+in^+, and ohmic n^+p^+ homojunctions (**Fig. 7.3**); and ohmic junctions between metal electrodes and heavily-doped p^+ and n^+ layers. Based on these doping techniques, a tandem organic solar cell was formed in a C_{60}:6T film by connecting two photoactive p^+in^+-homojunctions via a heavily doped n^+p^+-ohmic interlayer (**Fig. 7.4**). The value of V_{oc} and the conversion efficiency of the tandem cell reached 1.69 V and 2.4%, respectively.

The introduction of direct doping into bulk co-deposited films can provide the following improvements in the design of organic solar cells. (i) A built-in electric field can be constructed directly in the co-deposited region where the generation and transport of photocarriers occurs. (ii) A reduction of the bulk resistance of co-deposited films by doping can enable the growth of co-deposited films that are sufficiently thick (e.g. 1 μm) to absorb the whole of the incident solar light and to convert it to a photocurrent. Therefore, these doping techniques would significantly help in the development of an efficient organic solar cell.

7.2. Future prospects

The present doping techniques can be utilized for various material systems such as co-deposited films containing phthalocyanines, oligothiophenes, and C_{70}. In addition, precise energy-band mapping using a Kelvin probe would help us to optimize the cell design. The author believes that this doping technique will lead to the development of a 15% efficient organic solar cell. Moreover, the technique can be also applied to the fabrication of different devices such as organic transistors and organic light-emitting diodes.

List of Publications

1) Doping-based control of the energetic structure of photovoltaic co-deposited films

   Norihiro Ishiyama, Masayuki Kubo, Toshihiko Kaji, and Masahiro Hiramoto

   Appl. *Phys*. *Lett*., **99**, 133301 (2011).

2) Tandem photovoltaic cells formed in single fullerene films by impurity doping

   Norihiro Ishiyama, Masayuki Kubo, Toshihiko Kaji, and Masahiro Hiramoto

   Appl. *Phys*. *Lett*., **101**, 233303 (2012).

3) Tuning of Barrier Parameters of *n*-Type Schottky Junctions in Photovoltaic Co-Deposited Films by Doping

   Norihiro Ishiyama, Tadashi Yoshioka, Toshihiko Kaji, and Masahiro Hiramoto

   Appl. *Phys*. *Express*, **6**, 012301 (2013).

4) Tandem organic solar cells formed in co-deposited films by doping

   Norihiro Ishiyama, Masayuki Kubo, Toshihiko Kaji, and Masahiro Hiramoto

   Org. *Electron*., submitted.

5) Evaluation of *n*-Type Schottky Barrier Width for Photovoltaic Co-deposited Film by Low-frequency Capacitance Measurement

   Norihiro Ishiyama, Tadashi Yoshioka, Toshihiko Kaji, and Masahiro Hiramoto

   Mol. *Cryst*. *Liq*. *Cryst*., submitted.

List of Supplementary Publications

6) *pn*-control and *pn*-homojunction formation of metal-free phthalocyanine by doping

Yusuke Shinmura, Masayuki Kubo, **Norihiro Ishiyama**, Toshihiko Kaji, and Masahiro Hiramoto

AIP Advances, **2**, 032145 (2012).

7) Invertible Organic Photovoltaic Cells with Heavily Doped Organic/Metal Ohmic Contacts

Masayuki Kubo, Yusuke Shinmura, **Norihiro Ishiyama**, Toshihiko Kaji, and Masahiro Hiramoto

Appl. *Phys*. *Express*, **5**, 092302 (2012).

Poster Presentations in International Conferences

1) Doping-based control of the energetic structure of the co-deposited films

   Norihiro Ishiyama, Masayuki Kubo, Toshihiko Kaji, and Masahiro Hiramoto

   Plastic Electronics 2011, Messe Dresden, Germany, October 2011.

2) Doping-based Control of the Energetic Structure of the Co-deposited Films

   Norihiro Ishiyama, Masayuki Kubo, Toshihiko Kaji, and Masahiro Hiramoto

   2012 MRS Spring Meeting, Moscone West Convention Center, San Francisco, USA, April 2012.

3) Control of the energetic structure of *n*-type Schottky junctions in photovoltaic co-deposited films

   Norihiro Ishiyama, Tadashi Yoshioka, Toshihiko Kaji, and Masahiro Hiramoto

   KJF International Conference on Organic Materials for Electronics and Photonics 2012, Tohoku University, August 2012.

Oral Presentations in Conferences (in Japanese)

4) Energetic Structure Control of Co-evaporated Layer by MoO_3 Doping

   Norihiro Ishiyama, Masayuki Kubo, Toshihiko Kaji, Kai Iketaki, and Masahiro Hiramoto

   The 72nd Autumn Meeting, 2011 (The Japan Society of Applied Physics), Yamagata University, August 2011.

5) *pn*-Homojunction Formation in C_{60}:6T Co-evaporated Films

Norihiro Ishiyama, Masayuki Kubo, Toshihiko Kaji, and Masahiro Hiramoto

The 59th Spring Meeting, 2012, (The Japan Society of Applied Physics), Waseda University, March 2012.

6) Determination of Depletion Layer Width for Doped Junctions

Norihiro Ishiyama, Masayuki Kubo, Toshihiko Kaji, and Masahiro Hiramoto

The 59th Spring Meeting, 2012, (The Japan Society of Applied Physics), Waseda University, March 2012.

7) Tandem Cell Fabrication in Fullerene Single Films by Doping

The 73rd Autumn Meeting, 2011 (The Japan Society of Applied Physics), Matsuyama University, September 2012.

List of Books

1) Control of *pn*-Properties by Doping and Organic Thin-film Solar Cells

Masahiro Hiramoto, Masayuki Kubo, **Norihiro Ishiyama**, and Toshihiko Kaji, in: Yutaka Matsuo, Cutting-edge Research in Organic Thin-film Solar Cells, CMC Publishing, Tokyo, 2012, pp. 122-136 (in Japanese).

Acknowledgement

The author wishes to express his sincere gratitude to Professor Masahiro Hiramoto at The Graduate University for Advanced Studies for invaluable guidance, helpful suggestions, meaningful discussions, and continuous encouragement throughout this study.

The author makes grateful acknowledgement to Prof. Hiroshi Yamamoto, Associate Prof. Donglin Jiang, and Associate Prof. Toshi Nagata at The Graduate University for Advanced Studies and Prof. Masanobu Izaki at Toyohashi University of Technology for the review of this thesis.

The author would like to thank Assistant Professor Toshihiko Kaji and Dr. Iketaki for the helpful suggestion and discussion.

The author is grateful to Mr. Akira Adachi at Epi Tech Inc. and his associates for the cooperation on the development of equipment for a ‘three component co-evaporation’ technique.

The author thanks Associate Professor Takashi Sagawa at Kyoto University for the cooperation on the measurements of atmospheric photoelectron spectroscopy.

The author gratefully appreciates financial support from Core Research for Evolutional and Technology (CREST) from Japan Science and Technology Agency.

Grateful acknowledgements are given to the author’s co-workers, Mr. Masayuki Kubo and Mr. Tadashi Yoshioka for their helpful assistance and discussions. Finally, grateful acknowledgements are given to all the members of the research group under the direction of Prof. Masahiro Hiramoto at Institute of Molecular Science and CREST project team for their helpful assistance and friendship.